

Refill Friction Stir Spot Welding Of Dissimilar Alloys

by

Yuyang Chen

A thesis

presented to the University of Waterloo

in fulfillment of the

thesis requirement for the degree of

Master of Applied Science

in

Mechanical Engineering

Waterloo, Ontario, Canada, 2015

©Yuyang Chen 2015

Author's Declaration

I hereby declare that I am the sole author of this thesis. This is a true copy of the thesis, including any required final revisions, as accepted by my examiners.

I understand that my thesis may be made electronically available to the public.

Yuyang Chen

Abstract

Lightweight alloy materials such as magnesium and aluminum alloys are frequently employed in the automotive and manufacturing industry in order to improve vehicle fuel economy. This creates a pressing need for joining of these materials to each other, as well as to steels. Given the drastic difference in thermal and mechanical properties of these materials and the limited solubility of aluminum or magnesium in steel, dissimilar alloy fusion welding is exceptionally difficult. Refill friction stir spot welding (RFSSW) is a solid-state joining technology which connects two materials together with minimal heat input or distortion. The RFSSW process involves a three-piece non-consumable tool with independently controlled sleeve and pin components, which rotate simultaneously at a constant speed with the sleeve penetrating into only the top sheet.

Joining of Al 5754 alloy and DP 600 plate using friction stir seam welding is investigated. Two travel speeds of the shoulder are used to compare the mechanical and microstructural properties of the two kinds of welds made. Scanning electron microscopy (SEM) and optical microscopy are utilized to characterize the microstructure. Mechanical properties are evaluated using tensile testing.

Joining of Al 6063-T6 and Zn coated DP 600 steel using RFSSW is studied. Spot welds could reach a maximum overlap shear load of 3.7 kN when using a tool speed of 2100 RPM, a 2.5 s welding time and 1.1 mm of penetration into the upper Al 6063 sheet. Scanning electron microscopy (SEM) and energy-dispersive X-ray spectroscopy (EDX) were conducted to characterize the interface, which revealed that zinc layer was displaced into the interface and upper sheet, which may facilitate the bonding between the two sheets. Microhardness measurements reveal that the fracture path propagates through the soft heat affected zone of the Al alloy during overlap shear testing.

Joining of Mg alloys ZEK with Zn coated DP 600 steel sheets by RFSSW is also studied here. In joints between ZEK 100 and DP 600, the maximum overlap shear fracture load is 4.7 kN, when a 1800 RPM tool speed, 3.0 s welding time and 1.5 mm penetration into the upper ZEK 100 sheet is applied. SEM and transmission electron microscopy (TEM) revealed that a continuous layer of FeAl₂ particles accommodate bonding of the ZEK 100 and DP 600 sheets, which appears to have originated from the galvanized coating on the DP 600. If the zinc layer is removed then the maximum overlap shear fracture load is 3.1 kN. X-ray diffraction analysis of

the interface between the Mg alloy and the DP 600 steel on the Mg side also revealed that intermetallic (IMCs) such as FeAl_2 existed as an interfacial layer between the two sheets. It can be revealed from the displacement curve that the absorbed energy of the weld made under the condition of 1800 RPM, 3.5s, and 1.5mm of plunge depth in tensile testing up to failure point is approximately 2.73J.

Acknowledgements

I would like to thank my supervisors Prof. Adrian Gerlich and Prof. Michael Worswick for their continuous mentoring and support. I also want to thank my peers Jeff Hou and Zhikang Shen for their collaboration in this project and help in our daily work. The other thanks are given to my best group members for their support all the time, including our two lab technicians Mark Griffet and Dr. Yuquan Ding.

I would love to thank my family and genuine friends who always give me support in my decisions and life here in Canada.

This work has been supported by the Natural Sciences and Engineering Research Council (NSERC) of Canada, the Canadian Foundation for Innovation, Automotive Partnership Canada and the Ontario Research Fund. Support from Cosma International and HUYS Industries is also gratefully acknowledged. The focused ion beam (FIB) sample preparation for TEM research described in this paper was performed at the Canadian Centre for Electron Microscopy at McMaster University, which is supported by NSERC and other government agencies. The thesis describes work which is part of the Implementing Agreement on Advanced materials for transportation under the auspices of IEA.

Table of Contents

Author's Declaration.....	ii
Abstract.....	iii
Acknowledgements.....	v
List of Figures	viii
List of Tables	xi
Chapter 1: Introduction.....	1
1.1 Background.....	1
1.2 Friction stir welding	1
1.2.1 Introduction to friction stir spot welding	1
1.2.2 Industrial application of friction stir welding technology.....	3
1.2.3 Previous work on friction stir welding.....	5
1.2.3.1 Review of dissimilar metal joining using friction stir welding	5
1.2.3.2 Review of friction stir spot welding (FSSW).....	7
1.2.4 General review of FSW	8
1.2.5 Review of FSSW process.....	11
1.3 RFSSW and its advantages over FSSW	13
1.3.1 Microstructural formation of RFSSW	14
1.3.2 Mechanical formation of RFSSW.....	17
1.3.3 RFSSW of dissimilar materials	19
1.4 Motivation and Objective.....	23
1.5 Thesis layout.....	24
Chapter 2: Experimental Apparatus and Methods.....	25
2.1 Base material studied	25
2.2 Welding equipment.....	27
2.3 Mechanical Testing.....	29
2.4 Metallographic Analysis	30

2.5 Microhardness Testing	32
Chapter 3: FSW of Al 5754 to DP 600.....	33
Chapter 4: RFSSW of Al 6063 to DP 600.....	36
4.1 Influence of processing parameters on adhesion to the tool	36
4.2 Mechanical Properties	42
4.3 Summary.....	43
Chapter 5: RFSSW of ZEK 100 to DP 600	44
5.1 Interfacial Microstructure Investigation.....	44
5.2 Microhardness testing.....	52
5.3 Mechanical Properties	53
5.3.1 Tensile/shear Results of ZEK 100/DP 600 RFSSW Joints.....	53
5.3.2 Comparison of RFSSW of ZEK 100 to DP 600 with/out Zn coating and brush finished ZEK 100 to DP 600 with Zn Coating	55
5.4 Summary.....	56
Chapter 6: Conclusions.....	57
6.1 General conclusion of dissimilar materials by RFSSW results	57
6.2 Comparison of different materials RFSSW results	57
6.3 Future work	57
Appendix.....	58
1. Table 1: Base material compositions from chemistry analysis report [41]	58
2. AWS D8.1M:2007 standard.....	58
Reference	59

List of Figures

Figure 1: A typical micrograph of the friction stir weld cross-section in the welding direction [4].	2
Figure 2: Friction stir spot weld applied within the 2013 Honda Accord [11]	4
Figure 3: Illustration of the FSSW process: a. plunging, b. stirring, c. retracting [22]	8
Figure 4: Schematic illustrations for FSW in thin plates. A rotating (rotational speed, R) pin (HP) penetrates into the sheet at a transverse speed, T: (a) butt weld arrangement; (b) weld zone development by advancing the head pin into a continuous plate section [23].....	9
Figure 5: Optical microscope comparing (a), (b) the original aluminum alloy 1100 plate microstructure with (c) the friction-stir-weld nugget zone microstructure [23].....	10
Figure 6: TEM bright field images of the dynamically recrystallized grain structure within the friction-stir-weld nugget zone: (a) top of the nugget; (b) weld zone centre; (c) near the bottom of the weld [23]	11
Figure 7: Optical microscopy (OM) macrograph of a typical FSSW joint cross-section [24].....	12
Figure 8: Comparison of the weld surface from conventional (a) friction spot weld and (b) refill friction stir spot weld [36].....	13
Figure 9: Schematic of different stages of process by RPS100 spot friction welding system [36]	14
Figure 10: Optical micrographs of a typical RFSSW joint sectioned in the plunging direction showing the weld nuggets, metallurgical features and imperfections [24].....	15
Figure 11: Optical micrographs of RFSSW joints showing details of: (a) refined and equiaxed grains in the SZ; (b) highly deformed grains in the TMAZ; (c) larger grains in the BM [24]	15
Figure 12: Optical micrographs of RFSSW joints in Al 7075 alloy compared for different plunge depths and welding times [24].....	16
Figure 13: Optical micrograph indicating variation of grain size in the thickness direction in the centre of a RFSSW Al 7075 alloy joint (magnified) [24].....	16
Figure 14: Characteristics of hook feature at the periphery of the bonded interface with different processing parameters in RFSSW Al 7075 joints; arrows marked at the edge of unbonded region [24].....	17
Figure 15: Correlation between rotational speed and welding strength at different welding time in RFSSW AA6184-T4 joints [24].....	18
Figure 16: Optical microstructure of a friction spot weld between AZ31 similar sheets at the welding parameter of 1500 rpm, 2.75 mm of the penetration depth and 1 s of the welding time. (A) Bonding ligament and (B) hook [37]	18

Figure 17: Illustration of different failure modes observed under fracture test. (a) Through weld (2.25 mm of the plunge depth), (b) non-circumferential pull-out mode and (c) circumferential fracture mode (2000 rpm of the rotation speed). (U) Refers to the bottom.....	19
Figure 18: Correlation between lap shear strength and the length of the fracture sheet surface [37].....	20
Figure 19: Weld surface illustration after FSSW [38]	21
Figure 20: (a) Correlation between mechanical strength and welding time as well as tool rotational speed, (b) fracture surface through the interface at the condition of 1050 revolutions/min of the tool, 5 s of the welding time, (c) 1600 rpm revolutions/min of the.....	21
Figure 21: Macrostructure and Microstructure of the weld nugget [39]	22
Figure 22: Correlation between cross-tensile load and rotation speed [39].....	23
Figure 23: Friction stir welder (Jafo manual milling machine) [40]	27
Figure 24: RPS100 spot friction welding system	27
Figure 25: Welding parameters edit menu of refill friction stir spot machine	28
Figure 26: Schematic of Instron 4206 (Norwood, MA) tensile test machine [40]	30
Figure 27: Test coupon geometry and tensile shear test set-up [40]	30
Figure 28: JEOL JSM-6460 equipped with Oxford Instruments INCA-350 energy-dispersive spectroscopy system (left) and JEOL 2010 TEM/STEM is a field emission Transmission Electron Microscope (right) [40]	31
Figure 29: Optical micrographs of Al 5754/DP 600 weld produced at the travel speed of (a) 45 mm/min, and (b) 16 mm/min, (c) microstructure of steel directly under the tip of the pin [40].....	34
Figure 30: SEM micrograph of interface near the boundary of the stir zone, and (b) Al/Fe interface in the middle of the stir zone [40]	34
Figure 31: Correlation between fracture load and penetration depth of the pin into the steel [40]	35
Figure 32: Weld surface in RFSSW joints between Al 6063 and DP 600, produce using 1800RPM, 2.5s welding time and various plunge depths	37
Figure 33: Weld surface of refill friction stir spot weld of Al 6063/DP 600 under the condition of 1800rpm, 2s of dwell time, 1.1mm of plunge depth, 1.5s of retract time	38
Figure 34: Optical micrographs of RFSSW joint between Al 6063/DP 600 using (a) stereo microscope using indirect lighting and (b) compound metallographic microscope using incident light.....	39
Figure 35: Steel coating layer EDX mapping analysis	40
Figure 36: DP 600 coating layer EDX line analysis	40

Figure 37: Refined microstructure at the periphery of the stir zone from area A (left) and coarse grains in the heat affected zone from area B (right).....	41
Figure 38: (a) Outer periphery of Al 6063/DP 600 joint bonded region, and (b) high magnification image of the Al 6063/DP 600 interface	42
Figure 39: Tensile/shear results of Al 6063 and DP 600 at various welding conditions with the plunging depth uniform at 1.1mm	43
Figure 40: (a) weld surface appearance of ZEK 100/DP 600 joint and (b–d) optical micrograph of ZEK 100/DP 600 joint showing heavily deformed stir zone and bonded interface at condition of 1800 RPM/3 s, 1800 RPM/3.5 s and 2100 RPM/3 s.....	45
Figure 41: Grain structures in ZEK 100 stir zone produced using 1800 RPM and 3 s	46
Figure 42: Images (SEM) of ZEK 100/DP 600 joint	48
Figure 43: HAADF image (TEM) of interface with element maps for Al, Mg, Fe, O, C and Zn ...	49
Figure 44: High angular annular dark field image (TEM) of interface with element maps for Al, Mg, Fe, O, C, Zn, Si and Mn	50
Figure 45: Bright field image (TEM) and corresponding convergent beam electron diffraction pattern of second phase FeAl ₂ particle (noted by arrow) observed directly at the ZEK100/DP600 interface	51
Figure 46: X-ray diffraction pattern of overlap shear fracture surface on steel side	52
Figure 47: Microhardness profiles a across Mg alloy stir zone in ZEK 100/DP 600 joint when using parameters of 1800 RPM/3.5 s(Left) and along centreline of nugget traverse to interface at condition of 1800 RPM/3.5 s(Right).....	53
Figure 48: Tensile/shear results of ZEK 100 and DP 600 at various welding conditions with the plunging depth uniform at 1.5mm(Left); Tensile/shear results of ZEK 100 and DP 600 at various plunge depths when the tool speed is 1800RPM and welding time is 3 s(Right)	54
Figure 49: Tensile testing displacement curve of the weld made under the condition of 1800RPM, 3.5s, and 1.5mm of the plunge depth	55
Figure 50: Comparison of tensile/shear load between ZEK 100/DP 600, brush finished ZEK 100/DP 600, and ZEK 100/brush finished DP 600.....	56

List of Tables

Table 1: Base material compositions from chemistry analysis report.....	26
Table 2: Welding parameters and their range of quantity	29
Table 3: Detailed parameters and tool travel speeds during Al 6063/DP 600 welding	38

Chapter 1: Introduction

1.1 Background

Recently there has been an increasing focus on reducing the weight of automobile structures to reduce fuel consumption cost by improving fuel-efficiency. This has motivated the widespread use of lightweight alloys in transportation structures. However, since automotive structures remain largely steel-based, a core requirement for the application of lightweight alloys lies in dissimilar joining of magnesium and aluminum alloys to high strength steels. This has motivated the study of new joining processes for dissimilar material, especially solid-state welding techniques, which can avoid many of the issues such as excessive heat input, fume generation, cracking, and poor joint properties that are commonly encountered when fusion welding these combinations of nonferrous and ferrous materials. While aluminum and steel are not compatible during fusion welding, friction stir welding is seen as one of the most convenient techniques for joining various alloys as well as dissimilar metal combinations [1]. Friction stir welding (FSW) has already been broadly used for lap and butt welding in various industries for welding of aluminum alloys [2]. Refill friction stir spot welding (RFSSW) is an advanced version of friction stir welding which leaves no keyhole or indentation on the weld surface and provides a potential avenue for joining of dissimilar materials [3]. Although some studies have examined joining of aluminum alloys, limited work has been found that explores the microstructure and mechanical properties of RFSSW joints for dissimilar metal combinations; thereby, the present work examines the weldability of both Al alloys to steel, and Mg alloys to steel using RFSSW as well as the influence of welding parameters on the microstructure and mechanical performance of the joints.

1.2 Friction stir welding

1.2.1 Introduction to friction stir spot welding

Friction stir welding (FSW) was first invented and developed at The Welding Institute (TWI) in the UK in 1991, making it one of the newer welding processes to be used in practice. It is a solid-state joining technology which has been used to successfully weld aluminum and magnesium alloys, and high strength steels. FSW can be performed on a milling machine with a non-consumable rotating tool consisting of an inner pin and outer shoulder. The tool contacts

and penetrates into the abutting edges of the sheets being joined and traverses along the faying interface of the joint. While the tool rotates, it generates a large amount of frictional heat on the work piece. This heat softens the material surrounding the pin and facilitates movement of material flow around the pin to displace material from the front of pin to the backside of the rotating pin. Since no melting occurs in this process, the process was patented as a solid-state joining technology. The centre of the joint, the weld nugget, namely, stir zone (SZ), exhibits a size and morphology which depends on the size and geometry of the tool involved. In terms of the weld nugget microstructure, it is grouped into three features of the adjacent space, consisting of the stir zone, thermo-mechanically affected zone (TMAZ), and heat affected zone (HAZ) (Figure 1). In TMAZ, strain and temperature are lower and the effect of welding on the microstructure is correspondingly smaller. HAZ is subjected to a thermal cycle but is not deformed during welding. The temperatures are lower than those in the TMAZ but may still have a significant effect if the microstructure is thermally unstable. Due to the intense plasticization and elevated temperatures generated in the nugget, grain recrystallization and refinement typically occurs. In addition, these conditions will induce phase transformation to precipitates along the weld nugget, TMAZ and HAZ regions.

Zone I represents a selected region of HAZ. Zone II represents a region under the sleeve in the upper sheet. Zone III features a region under the sleeve in the stir zone. Zone IV represents a selected region of TMAZ.

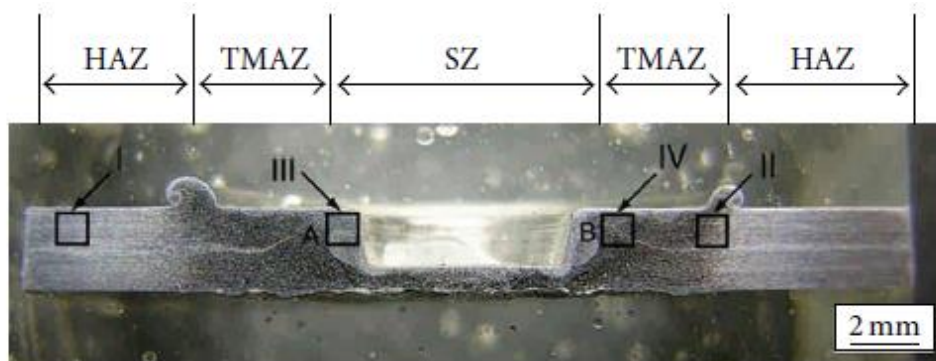


Figure 1: A typical micrograph of the friction stir weld cross-section in the welding direction [4]

Due to heavy material flow and plastic deformation, the refined and equiaxed grain structure in the nugget may enhance the strength of the material. In contrast, TMAZ will have a less

deformed structure as a result of lower heat generation which is not sufficient to refine the grain structure. Finally, the HAZ has a grain structure which is not affected by the heat, however in heat treated alloys it will exhibit coarsening of strengthening precipitates, which results in softening compared to the base material.

Overall, this relatively new technique is drawing more and more attention from the manufacturing industry, while also offering environmental benefits and high energy efficiency. The process requires no filler material during welding, such as wire, flux, or any other gases, and here is no generation of harmful fume emission. For instance, an aluminium/silicon filler wire generates by far the highest concentrations of ozone. Since no filler metal is used, almost any aluminum or magnesium alloy can be joined, thus avoiding the typical issues of compatibility encountered in fusion welding of different metals.

1.2.2 Industrial application of friction stir welding technology

Due to the fact that the automobile industry has been using more lightweight aluminum alloys, FSW has been used widely in this industry. In comparison with other fusion joining processes, using FSW to join dissimilar materials joining can lead to improvement of mechanical strength of the weld, especially for heat treated aluminum alloys. Nevertheless, further investigation is needed to optimize the parameters involved in the process. The following will review prior work on and applications of FSW in the automotive industry, the apparatus involved, and discussion of the process challenges and potential solutions.

The use of FSW for joining dissimilar metal combinations in the automotive and manufacturing industries has been studied widely. Honda has implemented friction stir welding in its 2013 Honda Accord, where cast aluminum and stamped steel in the engine cradle were connected by this technology (Figure 2) [7-9]. The strong interest is attributed to the fact that FSW offers a number of advantages for joining of dissimilar materials, including: enhanced mechanical properties of the joint (i.e. tensile and fatigue), improved process quality over the other joining technologies, and avoiding undesirable phase reactions which may occur when dissimilar metals melt at high temperature [5-6]. In the automotive industry, the focus on the implementation of FSW has mainly involved: larger extruded sheets made from being friction stir welded by each extruded part; tailored joint blanks made from being friction stir welded by sheet material; and lightweight alloys welding. Cost for each of the implementation has dipped due to

friction stir welding in comparison with the other welding technologies. Nevertheless, further investigation is needed to explore the possibility of dissimilar materials friction stir welding.

There is one key benefit of using FSW, which is that it is essentially a solid-state joining technology that has no melting happening in the welding process. Melting of alloys such as aluminum and magnesium alloys at elevated temperature will result in more formation of brittle intermetallic compounds (IMCs), which deteriorates mechanical joint strength by propagating fracture through the IMCs formation path. At lower temperature, distortion can be avoided and residual stress which can lead to the fracture of the joint will be reduced.

For example, Chen and Kovacevic [10] pointed out that the maximum temperature in dissimilar FSW of Al/steel is 631°C on the steel side, which is much lower than that as high as 1000°C in fusion welding. This reduction will limit the thermal stresses in FSW joints compared to fusion welding, and thus made it a feasible process for the Al/steel assembly in the 2013 Honda Accord, as shown in Fig. 2.

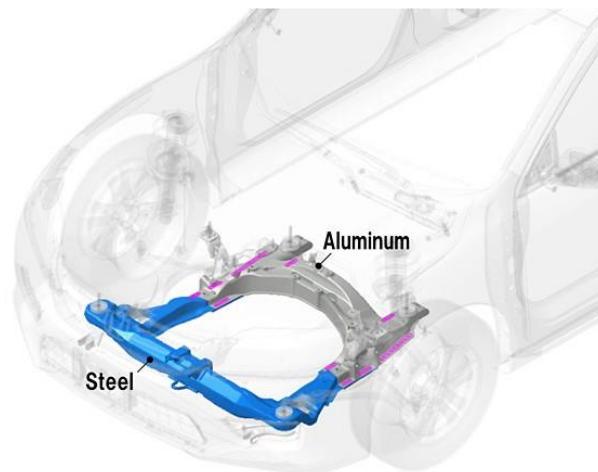


Figure 2: Friction stir spot weld applied within the 2013 Honda Accord [11]

In order to provide a high degree of flexibility in production, FSW may be conducted using an industrial robot. However, for many material and thickness combinations, typical industrial robots lack sufficient stiffness to conduct FSW. Nevertheless, previous work from Tower Automotive has proven that a relatively cheap robotic machine (ABB IRB 6400) can be used for FSW to join aluminum 6061-T6 [9]. This robot is able to produce welds in Al 6061-T6 with up to 4mm in thickness and travel speed of 1 m/min. Higher travel speeds can be accomplished when lower material thickness is joined. In order to compensate for the compliance of the 6-axis robot,

a force-controlled algorithm was developed that allows the robotic structure to resolve the stiffness contribution and correct for the compliance in real time. However, in terms of mass production in industry, this solution still limits the possible forces which can be applied and much higher stiffness robots are still needed for most FSW applications.

In conclusion, FSW is a promising joining technology which can replace other joining technologies, although some limitations and drawbacks remain in terms of possible applications in industry. FSW offers refined microstructure, little brittle intermetallic formation path and environmental benefits from which it can be concluded that this process has great potential for adoption in coming years.

1.2.3 Previous work on friction stir welding

1.2.3.1 Review of dissimilar metal joining using friction stir welding

As mentioned earlier, there is a pressing need for design engineers to join dissimilar materials for tailor-designed new structures or parts. Joining of dissimilar materials can bring the advantages of both materials to one structure, such as corrosion resistance in one material, and elevated temperature strength in the other material. In the case of most automotive designs which are dominated by steel, replacing components with aluminum or magnesium materials will require joining these alloys to steel.

Friction stir welding is taken as one of the greatest development in dissimilar materials joining and is a green technology due to its environmental benefits and energy efficiency [10]. Specifically, there is less consumable materials cost, such as flux, or shielding gases and no harmful emissions are generated [10]. This technique never requires any use of filler metal and thereby any aluminum or magnesium alloy can be joined while fusion welding has an issue with maintaining compatibility of filler metals. Moreover, as low as 2.5% of the same energy required for laser joining technique is consumed in FSW which offers efficiency during production [10].

Joining dissimilar materials is normally more difficult than joining similar materials since other factors influence the quality of a dissimilar materials joint, such as different thermal expansion coefficient of dissimilar materials, and formation of brittle intermetallic compounds which may lead to cracking. It may be possible to apply preheating to minimize thermal stresses during welding and cooling, however this may also further promote intermetallic formation [10].

The industrial application of FSW technology can be categorized into three branches, which contain the welding of extrusions to assemble an upsized profile, joining of customized joint parts, and joining for automobile assembly parts. For each of these branches, welding configuration varies significantly. For the first one, two standard joint configurations are used frequently, which are partial plunging butt and lap joint configurations, as are the most applied and capable of overcoming process variations in mass production; for the second branch mentioned, complete plunge weld is required. It should be noted, all of these categories have improved on travel speeds over the years, now reaching up to 2 m/min, making it feasible for mass production [12].

Although FSW has been applied to Al/steel joints in production of the 2013 Honda Accord, only a few studies are available which focus on this method [13]. There are three significant welding parameters in friction lap welding, tool rotation speed, travel rate, and tool shape. Moreover, pin length and its plunging depth into the lower sheet also has an impact on the weld strength. For example, when aluminum or magnesium alloys are joined to steel, the pin penetration into the steel will rapidly wear away steel-based tools, and, to avoid this one may maintain the pin above the sheet in order to promote diffusion bonding between the sheets [14].

Diffusion of different alloy elements could be one of the bonding mechanisms which facilitate the joining of dissimilar alloys with tool pin staying about 50 microns above the lower sheet surface [14]. One advantage of this bonding mechanism is the disruption of any formation of an intermetallic compound layer at the interface. To be noted, mechanical interlocking with deformation of lower sheet bending upwards into the upper sheet also plays a significant part in joining of the two sheets [14].

It can also be difficult to maintain this small distance between the tool pin and the lower sheet steel surface. However, when a tungsten (W) based tool is used, the tool may penetrate into the steel sheet during joining without encountering severe wear. In prior work by Chen and Nakata [15], the influence of tool penetration was considered in Mg/Steel FSW joining and it was shown that a thin interfacial reaction zone could be promoted when new layer of steel is exposed by the tool. Deformation of the steel sheet during tool penetration will also promote mechanical interlocking, which will contribute to joint strength [16]. However, this method will also promote formation of intermetallic compounds when aluminum and steels alloys are joined. This may result in cracks, joints that have high hardness, and thus limits joint strength [17, 18, and 19].

To date, only one prior study has considered the application of RFSSW to join aluminum to steel. It was reported by Verastegui *et al.* that sound RFSSW joints between AA 6181-T4 aluminum and DP 600 (dual phase steel with 600 MPa minimum tensile strength) steel sheets could be successfully produced [42]. The study involved steel sheet which was in two different surface conditions: with and without a galvanizing zinc surface layer. The results of lap shear tests showed that the galvanized layer does not cause a substantial change on the final joint strength, even though different joining mechanisms had been observed with and without the surface layer.

Prior work concerning diffusion bonding has revealed that mechanical strengths of the welds deteriorate with decreasing thickness of the intermetallic compound layer. For instance, it has been proven that joint strength dips heavily when the intermetallic compound layer exceeds 1.5mm [20]. Based on this, it seems that the FSW technique offers great potential in improving the joint strength between dissimilar alloys due to lower heat input prohibiting intermetallic compound layer from growing between the two welding sheets being joined.

1.2.3.2 Review of friction stir spot welding (FSSW)

As a derivative of FSW, FSSW can be used to produce a spot weld and shows great potential as a replacement for spot joining processes such as resistance spot welding and riveting.

Conventional FSSW was invented by Mazda Motor Corporation in 1993 [21]. As shown in Fig. 3, the FSSW process consists of three stages: contact, penetrating, and retracting [22]. The welding procedure initiates with the sleeve and pin spinning simultaneously at a constant speed. Then the tool plunges into the work pieces and touches the weld surface. The plunging movement of the tool causes displacement and mixing of both materials. After plunging, the stirring stage starts when the tool reaches a desired depth.

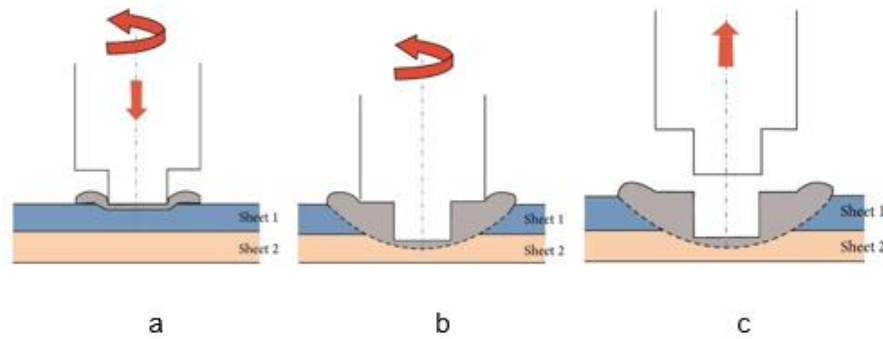


Figure 3: Illustration of the FSSW process: a. plunging, b. stirring, c. retracting [22]

There is significant friction generated in the contact and penetrating stage, and thereby alloys underneath and around the tool are heated up, softened, and mixed such that a solid-state joint will be formed. When a joint is obtained, the tool is retracted from the work pieces. This joint appears with a keyhole in the middle, which degrades the mechanical performance of the welds [22].

Due to the severe movement in the welding material, the stir zone undergoes heavy plastic deformation and recrystallization; thereby, original grains are transformed into much finer and equiaxed ones, which leads to the good mechanical performance of friction stir welded sheets. While the thermo-mechanically affected zone has bigger grains in a highly deformed structure, due to the moderate friction heating and deformation; the HAZ has coarser strengthening precipitates and grain sizes in comparison to base metal in the welding thermal cycle.

1.2.4 General review of FSW

Murr et al. [23] explored the dynamic recrystallization of friction stir welded joints in commercially pure Al 1100 thick plates. A range of head pin rotational speeds (R in Fig. 4) and transverse velocities (T in Fig. 4) were investigated, both for joining two pieces and for processing a single continuous section.

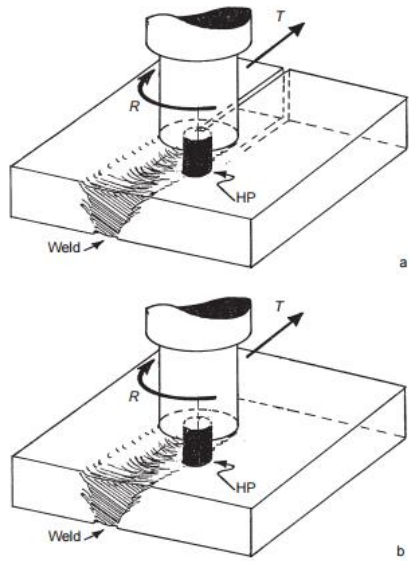


Figure 4: Schematic illustrations for FSW in thin plates. A rotating (rotational speed, R) pin (HP) penetrates into the sheet at a transverse speed, T: (a) butt weld arrangement; (b) weld zone development by advancing the head pin into a continuous plate section [23]

Fig. 5 shows images of microstructure of the original aluminum alloy 1100 plate and the friction-stir-welded nugget zone. It is apparent from Fig. 5 that the nugget zone microstructure (See Fig. 5 (c)) is significantly different and reduced in size from the large initial plate (See Fig. 5 (a, b)). Fig. 5(c) illustrates the dynamic recrystallization in magnified views of these microstructures for comparison with the base metal microstructure in Fig. 5(a, b). The dynamic recrystallization feature of the nugget zone is shown in Fig. 5(c) which exhibits generally equiaxed grains. As shown from the transmission electron micrographs in Fig. 6, the grain size was slightly smaller near the nugget bottom (Fig. 6c), where, in previous work [23], temperatures tended to be slightly lower than those under the weld surface.

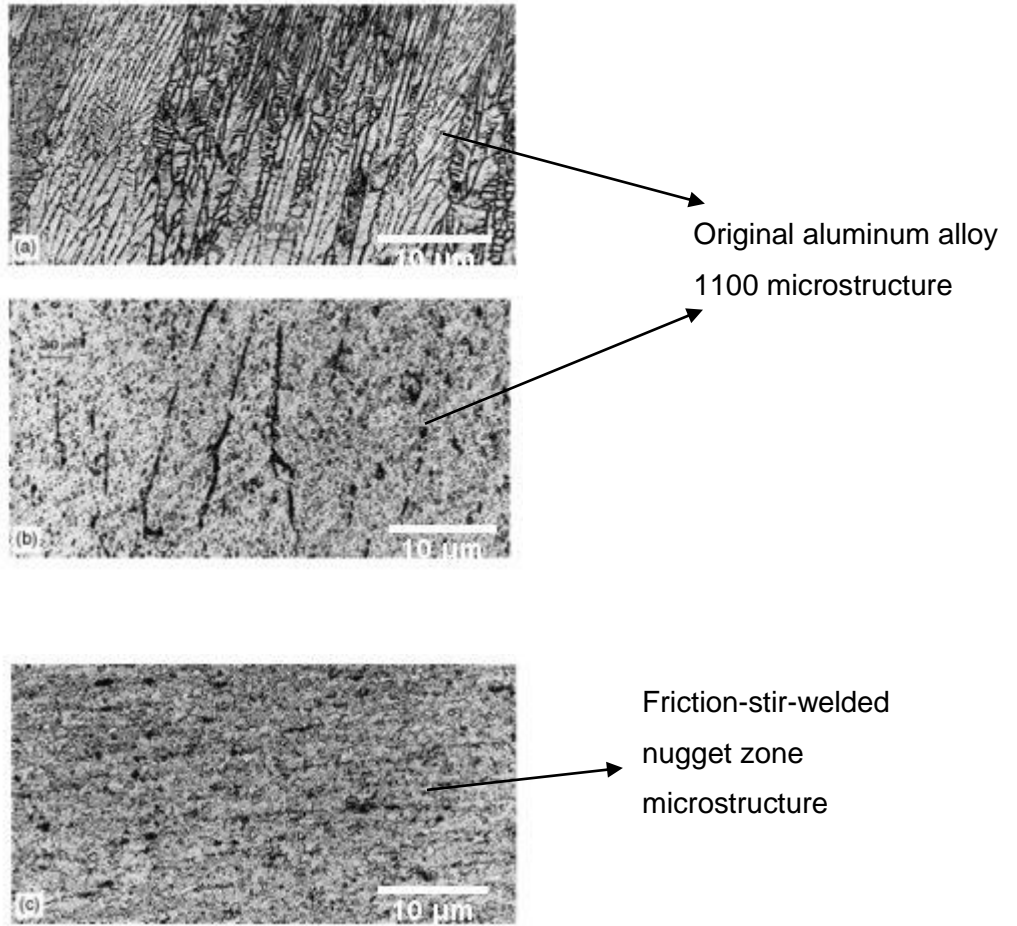


Figure 5: Optical microscope comparing (a), (b) the original aluminum alloy 1100 plate microstructure with (c) the friction-stir-weld nugget zone microstructure [23]

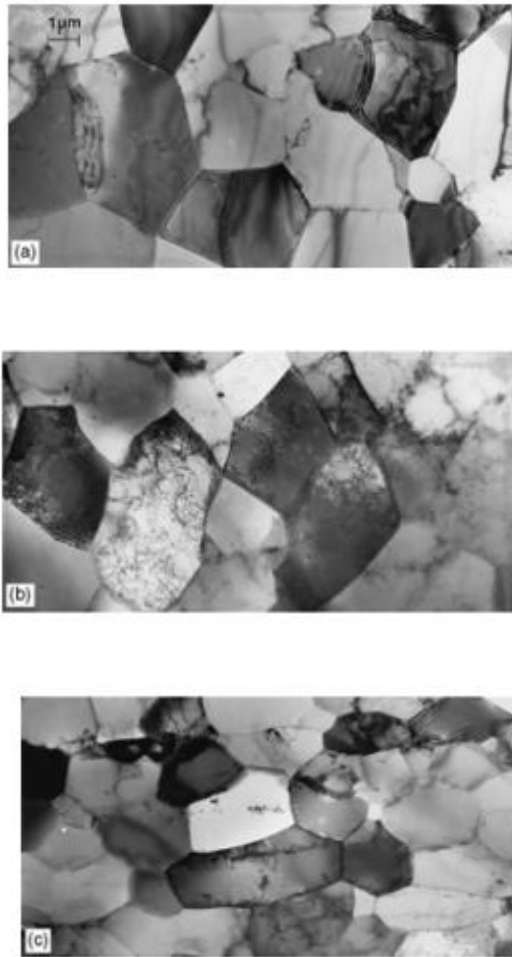


Figure 6: TEM bright field images of the dynamically recrystallized grain structure within the friction-stir-weld nugget zone: (a) top of the nugget; (b) weld zone centre; (c) near the bottom of the weld [23]

1.2.5 Review of FSSW process

The process begins with the tool rotating at an elevated speed. Then the tool is forged into work pieces until the tool shoulder contacts the top surface of the upper work piece to form a weld nugget. The plunging movement of the tool brings displacement of the materials. After plunging, the stirring stage starts when the tool reaches a desired depth.

The typical metallurgical zones of FSSW weld are referred to as the hook, partial bonding, and bonding ligament zones (Fig. 7) [24]. The hook zone has the shape of an upside down V; the partial bonding is the area in which the connection between the two sheets is not as strong as

the other bonding zone in the shape of a discontinuous line in the weld; the zone of bonding ligament presents the band structure due to material flow and the plunging force in the joint [24, 25]. Shen et al. [26] attributed the banded structure to incorporation of Al clad into the joint, while the lower sheet bends upward. Many scholars have investigated the hook feature around the interface between the two sheets [26, 27, and 28]. Yuan et al. [28] attributed it to incomplete break-up of oxidation film of aluminum. Others attributed it to poor flow ability of the materials and insufficient pressure from the tool [26]. Badarinarayan et al. [27] showed that the hook made with a cylindrical pin went gradually upward, while the hook made with a triangular pin ended near the stir zone.

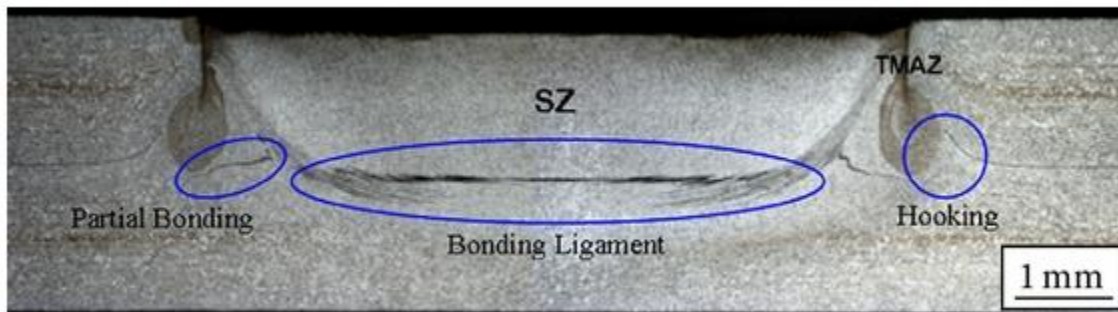


Figure 7: Optical microscopy (OM) macrograph of a typical FSSW joint cross-section [24]

As mentioned above in FSW, the Stir Zone (SZ) has fine equiaxed grains due to dynamic recrystallization [23, 30, 31, and 32]. The grain size in the SZ becomes larger with an increase of rotation speed [32] and is also controlled by the shape of tool. It was concluded that a triangular pin led to a finer grain size than a cylindrical pin [27, 32]. Sun et al. [29] reported that the SZ had low dislocation density because of heavy recrystallization. In the entire SZ of AZ31 and AM60 welds, Yamamoto et al. [30] observed fine equiaxed alpha-Mg grains which had diameters $<10\ \mu\text{m}$. Shen et al. [26] investigated refill FSSW of AA7075 and found that the hardening precipitation within the stir zone was either dispersed or broken into smaller particles by the tool movement. The grains near the tip of the pin and sleeve were finer than those in the centre of the nugget because the grains near the sleeve area were stirred more severely and were thus under more stress than the other regions.

With the increasing demand for reducing automobile weight to be fuel-efficient in order to trim cost and reduce emissions, Mg and Al alloys have been employed in body structures of cars as

light weight replacements for traditional steels. According to the research conducted by M. Yamamoto et al. [30], dissimilar friction stir welds were successfully made between magnesium and aluminum alloy sheets. It was found that the top surface of the weld became more integral and better quality with an increase in rotational speed. Y. Yan et al. [31] pointed out that friction stir welding between Al 5052 and AZ31 alloy with 6mm in thickness was successfully made. The microstructure of the stir zone revealed refined equiaxed grains.

The TMAZ underwent built-up frictional heat and shear deformation which resulted in highly deformed grains [33]. However, recrystallization was not observed in the case of TMAZ of AA7075 refill FSSW due to insufficient deformation on account of relatively low rotational speed and lower temperature than the SZ [26]. The heating rate of FSSW was fairly fast, which limited the dissolution of second phase particles in the TMAZ [35]; consequently Yin et al. [34] observed α -Mg grains for AZ31 weld. Similar results have been found in AZ91 FSSW welds [30].

The HAZ only experienced a welding thermal cycle, which caused the coarser grains [30]. For the refill FSSW joint of AA7075, the HAZ had coarser strengthening precipitates than those in the base metal [26].

1.3 RFSSW and its advantages over FSSW

Refill friction stir spot welding is an advanced derivative of conventional FSSW in which a “refill step” in the welding process is added after the FSSW process to eliminate the pin hole (Fig. 8). The refill FSSW, which connects two or more sheets of material in the lap configuration, was developed and patented by GKSS in Germany.

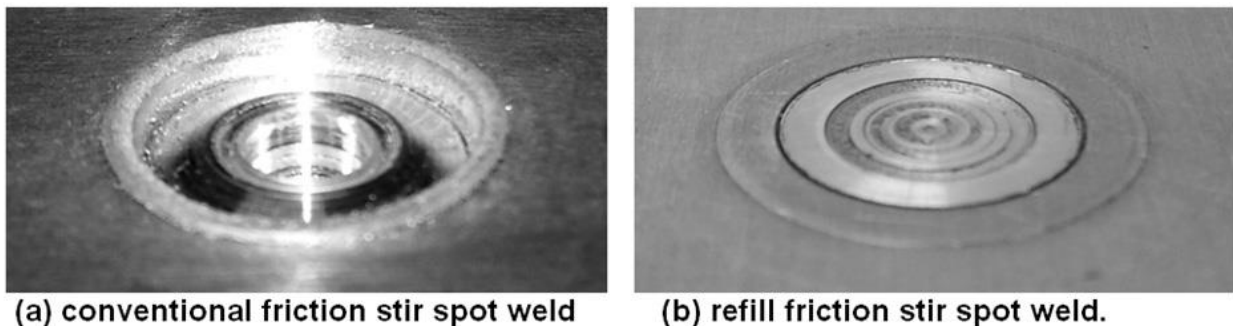


Figure 8: Comparison of the weld surface from conventional (a) friction spot weld and (b) refill friction stir spot weld [36]

Typically, RFSSW process involves the following four steps (see Fig. 9). First of all, the stationary clamping ring goes down to hold the work piece in the correct position during welding. In the meantime, the sleeve and pin are spinning at a certain revolution speed and plunged into the welding sheets to frictionally preheat the work piece. When the work piece is sufficiently preheated and begins to become plasticized, the sleeve proceeds to penetrate to the interface between the two sheets. In the meantime, the pin is retracted to leave certain space to displace the plasticized material. In the last refill step, the sleeve retracts, and the pin sticks out to inject the plasticized material back into the weld space.

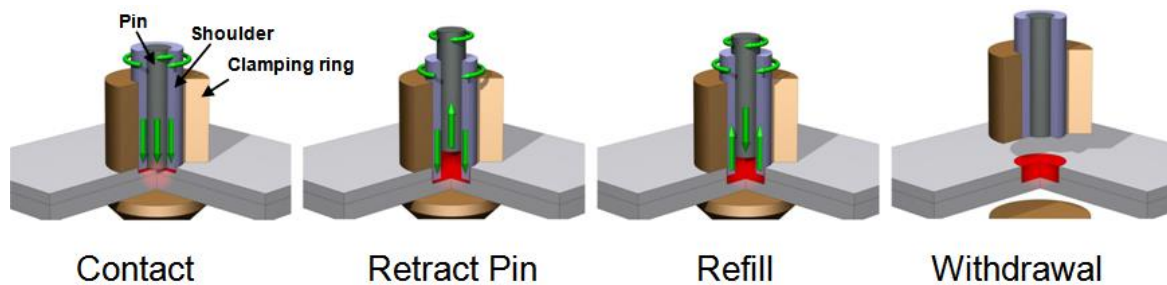


Figure 9: Schematic of different stages of process by RPS100 spot friction welding system [36]

Due to the refill step, this specific technique makes welds with no indentation on the weld surface or material loss (Fig. 8 (b)). The nugget space consists of material that has been plasticized from heavy material flow by the sleeve movement and solidified after cooling, ensuring a consolidated joint which has no loss of material in comparison to the original sheet surface [5].

1.3.1 Microstructural formation of RFSSW

RFSSW experiments have been performed by Rosendo et al. [24] in an Al 6181-T4 alloy to obtain a spot weld with no keyhole using varied joint parameters such as dwell time and rotational speed. Microstructural formation within the RFSSW joints was analysed by optical microscopy. The investigation of the welding sample showed physical and metallurgical patterns: hook, partial bonding and bonding ligament (see Fig. 10). The partial bonding is a transformed space where the bonding between the upper and lower sheets is not as strong. The bonding ligament is a relatively softer zone in comparison to the other areas around the interface, which might result in fracture degrading the mechanical strength.

Some defects in relation to the flow of the welding material were also seen in some spot welds, relying on the welding parameters. The deficient features were named “lack of mixing” and “incomplete refill” [24].

The TMAZ features heavily deformed grains compared to those in the base material and heat affected zones. The stir zone microstructure is featured by highly plasticized equiaxed fine grains as shown in Fig. 11(b). This microstructure is caused by dynamic recrystallization due to the high spinning speed during the penetrating step and heat input by the process [35].

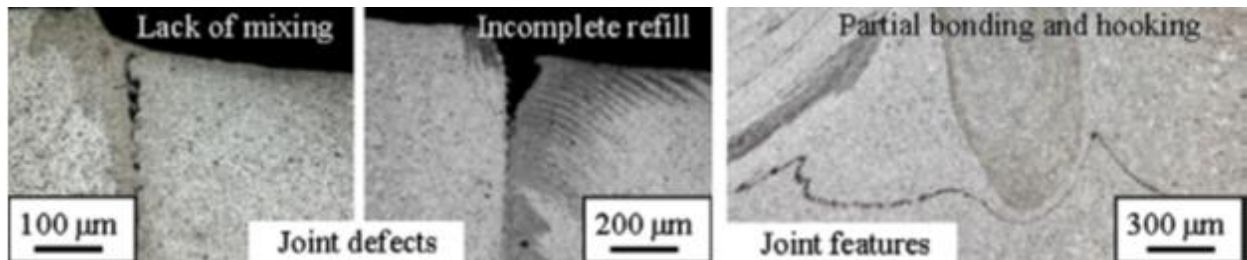


Figure 10: Optical micrographs of a typical RFSSW joint sectioned in the plunging direction showing the weld nuggets, metallurgical features and imperfections [24]

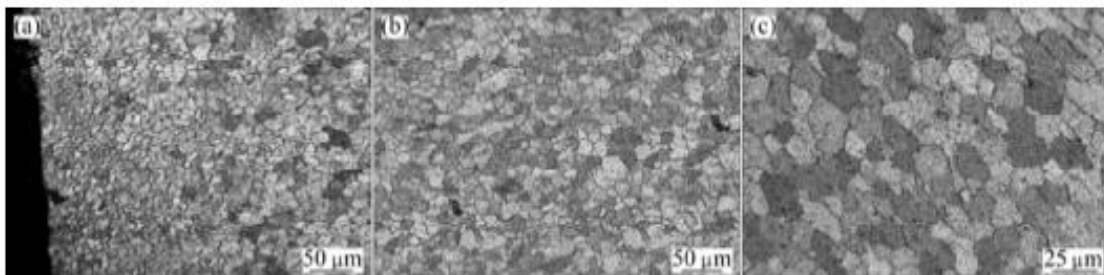


Figure 11: Optical micrographs of RFSSW joints showing details of: (a) refined and equiaxed grains in the SZ; (b) highly deformed grains in the TMAZ; (c) larger grains in the BM [24]

After the above, refill FSSW lap experiments were performed. The cross-section of the weld was made, which exhibits a bowl shaped plug appearance because the majority of the welding process occurs in the upper sheet. The weld can be separated into four parts according to the grained features of the welds, namely, stir zone, thermo-mechanical affected zone, heat affected zone and base metal. Fig. 12 shows that overall, the nugget thickness increases with longer welding time and more plunging depth due to more material being penetrated by the tool, and undergoing heating and dynamic recrystallization.

As shown in Fig. 13, variations in the grain size can be noted along transverse thickness direction. These grains are elongated in the horizontal direction because of the plunging downward force of the tool, and the grain sizes are much larger near the interface around the centreline, in the zone highlighted by the red line in Fig. 13. As shown in Fig. 14, there are also other features such as a bonding ligament and hook (marked as F), which will be discussed in detail below. As indicated in Fig. 14, the hook exhibits a slant V shaped appearance and is surrounded by fine equiaxed grains. Overall, the geometry of the hook becomes much sharper with less welding time and plunge depth [24].







	3 S	3.5 S
0.85 mm	 Average stir zone thickness: 725 μm	 832 μm
0.95 mm	 865 μm	 903 μm
1.1 mm	 967 μm	 1023 μm 1 mm

Figure 12: Optical micrographs of RFSSW joints in Al 7075 alloy compared for different plunge depths and welding times [24]

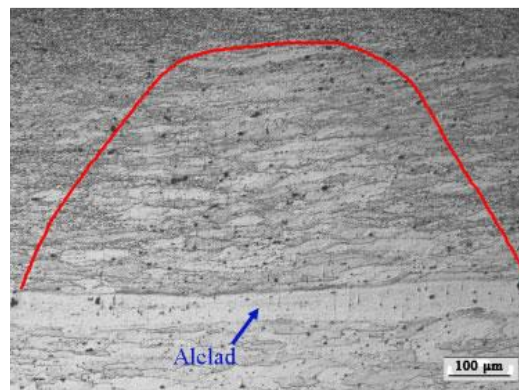


Figure 13: Optical micrograph indicating variation of grain size in the thickness direction in the centre of a RFSSW Al 7075 alloy joint (magnified) [24]

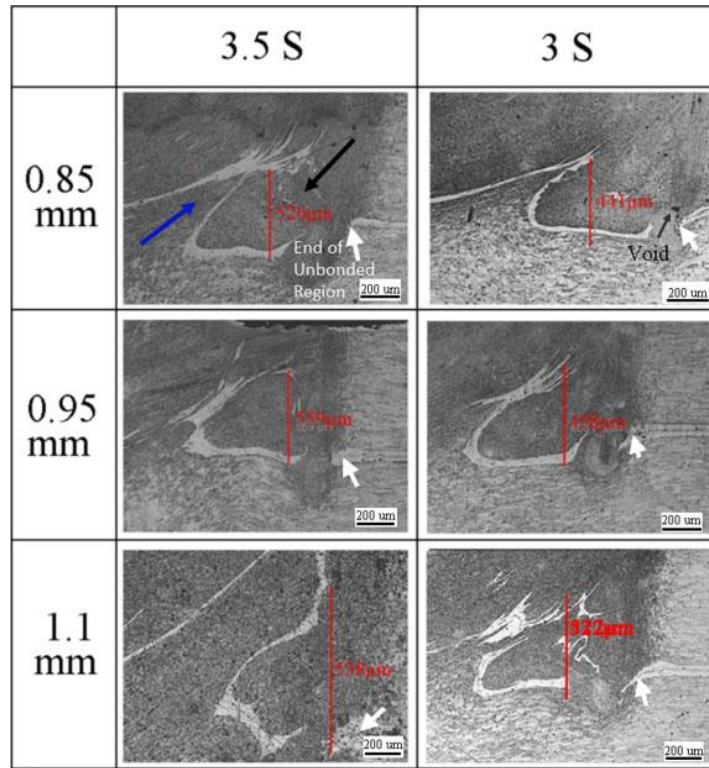


Figure 14: Characteristics of hook feature at the periphery of the bonded interface with different processing parameters in RFSSW Al 7075 joints; arrows marked at the edge of unbonded region [24]

1.3.2 Mechanical formation of RFSSW

The shoulder and pin are controlled by two separate actuators so that they move up and down independently of each other. However, they are controlled by one shared spindle so that they rotate simultaneously with each other. As the rotational speed becomes higher, more frictional heat is generated in the work piece. The plunging depth depends on the motion of the shoulder forging down into the welding work piece. There is more mechanical interlocking and deformation with increasing plunging depth. Lastly, with more welding time, more frictional work is generated to increase the frictional heat in the welding work piece.

The highest failure load of the experiment at different rotational speeds showed inconsistent trends at two different welding times, as illustrated in Fig. 15. Specifically, at the condition of 2.6s, fracture load diminishes when rotational speed goes up. On the other hand, there is no clear correlation between rotational speed and welding strength when the welding time is set as

3s. However, the fracture load also doubles when the dwell time increased from 2.6s to 3s at a constant tool rotation speed of 2400 RPM [24].

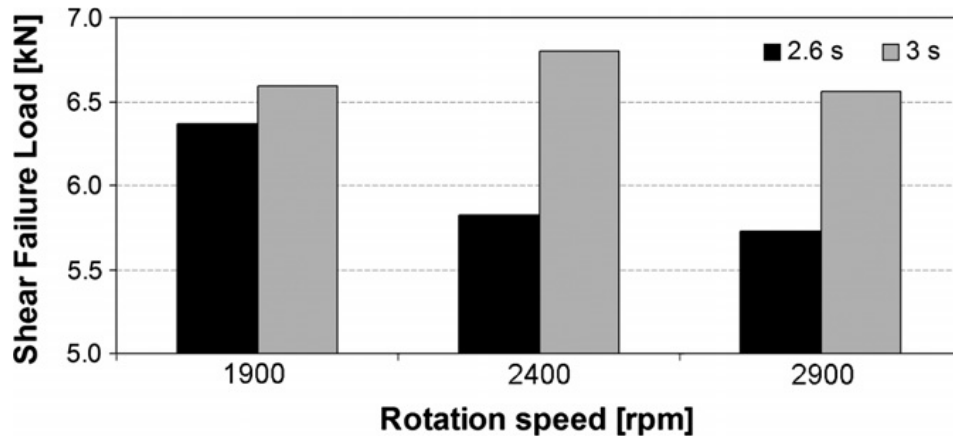


Figure 15: Correlation between rotational speed and welding strength at different welding time in RFSSW AA6184-T4 joints [24]

Campanell et al. studied the potential of joining AZ31 magnesium alloys using refill friction stir spot welding. Welds with the highest failure shear load were obtained with the combination of parameters that contribute to the most material mixture, longest metallurgical bonding, and minimal vertical displacement of hooks [37]. A macrograph of the stir zone is presented in Fig. 16, along with higher resolution micrographs of metallurgical patterns: bonding ligament (A) and hook regions (B). The bonding ligament is characterized as including voids or cavities along its propagating direction. A rise in the welding mechanical strength was shown to occur as the bonding ligament becomes larger.

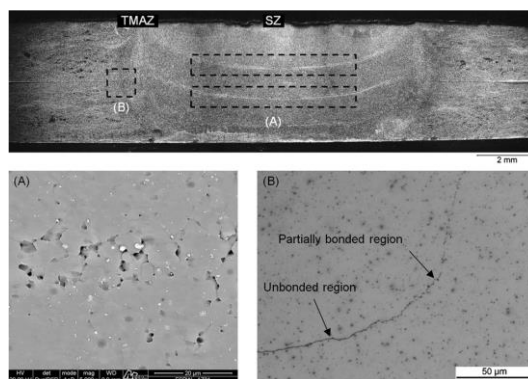


Figure 16: Optical microstructure of a friction spot weld between AZ31 similar sheets at the welding parameter of 1500 rpm, 2.75 mm of the penetration depth and 1 s of the welding time. (A) Bonding ligament and (B) hook [37]

It is revealed that three main fracture modes happened after tensile/shear testing, two being non-circumferential pull-out fracture modes and one circumferential pull-out fracture mode. No interfacial failure was found in this case, which proved that the welds in this experiment turned out to have high quality and strength (Fig. 17). From the fracture modes observed in Fig. 17, it can be seen that high deformation of the material out of plasticization resulted from high strain rates by the sleeve movement. Different stress and strain distribution determined the geometry of the hook and bonding ligament, which were some of the defects resulting in the fracture propagation [37].

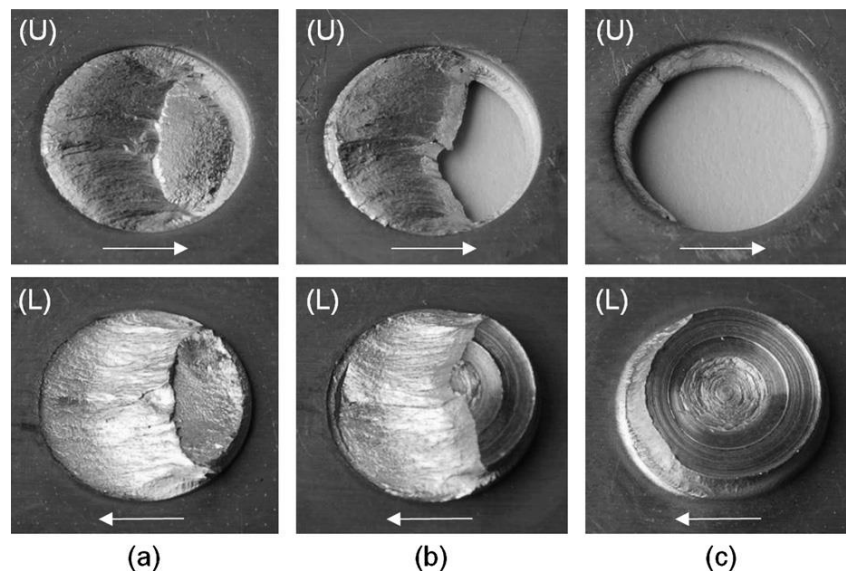


Figure 17: Illustration of different failure modes observed under fracture test. (a) Through weld (2.25 mm of the plunge depth), (b) non-circumferential pull-out mode and (c) circumferential fracture mode (2000 rpm of the rotation speed). (U) Refers to the bottom

1.3.3 RFSSW of dissimilar materials

The challenge of joining lightweight materials not only lies in similar materials, but also in dissimilar materials such as aluminum alloys and steels, aluminum alloys and magnesium alloys, and magnesium alloys and steels. Refill friction stir spot welding between Al 5754 and AZ 31 was conducted by Campanelli et al. [37]. Fig. 18 shows the influence of different welding parameters on the joint strength.

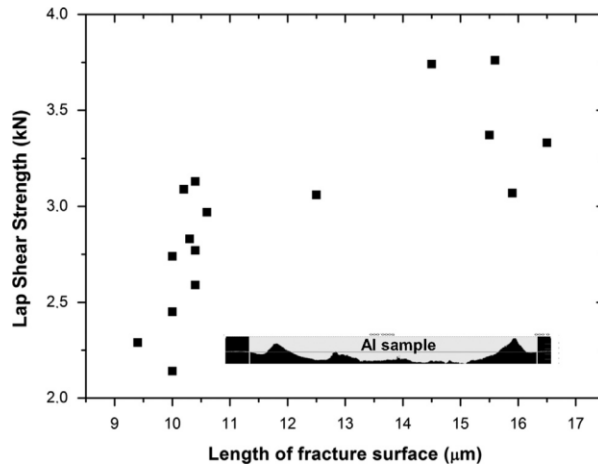


Figure 18: Correlation between lap shear strength and the length of the fracture sheet surface [37]

It is observed that non-circumferential pull-out fracture mode was the only one accountable for the fracture. It is inferred that fracture propagates from the defects through the brittle IMCs formed between aluminum and magnesium sheets.

It was found that $Al_{12}Mg_{17}$ and Al_3Mg_2 were distributed at the interface of the weld between two sheets as intermetallic compounds. The reason behind this distribution was that the material flow triggered by the tool motion lead to the element diffusion between two sheets.

Friction stir spot welding between aluminum plate and magnesium plate was investigated by Choia et al. [38] using various welding parameters to explore the effects of the welding parameters on the weldability of Al and Mg sheets. Multiple characterization techniques were utilized such as optical microscopy, scanning electron microscopy, and X-ray diffraction analysis to study the microstructure and intermetallic compounds at the interfacial area. Failure tensile testing was used to evaluate the mechanical properties of the welds. The results showed that intermetallic compounds were detected at the interface, the thickness of which increased as the rotational speed and welding time went up. With the thickness of intermetallic compound layer increasing, the tensile strength of the welds degraded heavily.

The weld surface of the joint was shown in Fig. 19 [38]. From Fig. 20, it can be shown that a sound joint between the two sheets was established by refill friction stir post welding. It also displayed that tensile strength degraded with the rise in the welding time. It was revealed that the fracture propagated through the intermetallic compound layer, the thickness of which

increased with the rise in welding time. A typical interfacial fracture was observed in nearly all the joints, as illustrated in Fig. 20(b) and (c).

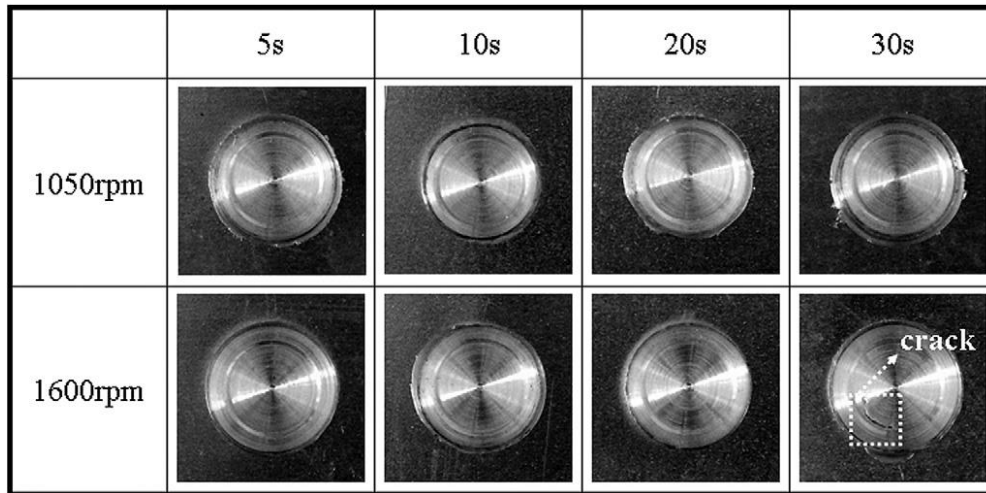


Figure 19: Weld surface illustration after FSSW [38]

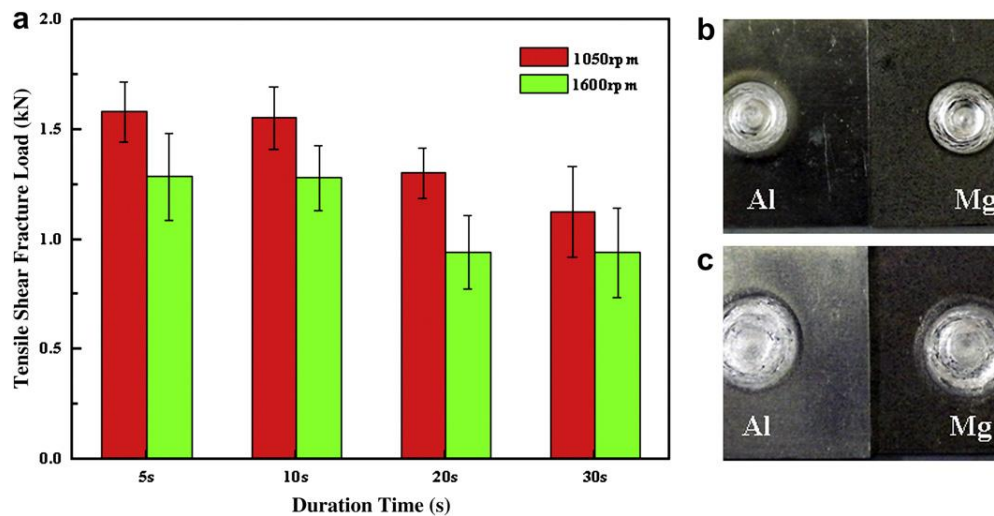


Figure 20: (a) Correlation between mechanical strength and welding time as well as tool rotational speed, (b) fracture surface through the interface at the condition of 1050 revolutions/min of the tool, 5 s of the welding time, (c) 1600 rpm revolutions/min of the

Mubiayi et al. [39] discussed the microstructure, defects, mechanical performance and fracture characteristics of friction spot welded joints of 2 mm thick dissimilar aluminum alloys (AA2024-T4 and AA5052-H112) .

It was found that Al 2024-T4 is coated with pure aluminum on its surface to protect it from oxidation, which can be stirred into the welds with the movement of the pin and sleeve along with a layer of oxides on its surface. The entrapped pure aluminum led to a softened zone termed as bonding ligament (see in Fig. 21), which is similar to inclusions in fusion welding.

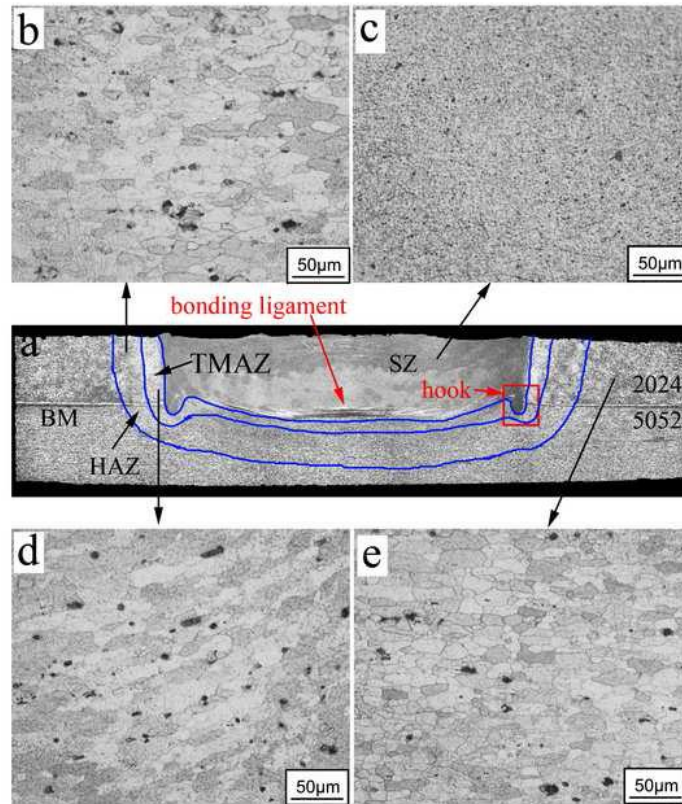


Figure 21: Macrostructure and Microstructure of the weld nugget [39]

In terms of mechanical properties, Fig. 22 shows the tensile strength profile for these joints [39]. At 1200 rpm of the rotational speed, the tensile load increases with more dwelling time. The factors involved are hook morphology and the bonding ligament distribution. With a increase of dwelling time, the U-shaped hook contains more area with longer processing time and more material volume. At the welding times of 4s and 5s, it was found that the tensile strength increased with the increase of rotation speed due to the fact that the grain size was more heavily refined at higher rotational speed. However, at the welding time of 6s, tensile strength dropped with the increase of rotation speed. This might be attributed to the fact that there was over heating at some areas leading to some cracks or defects.

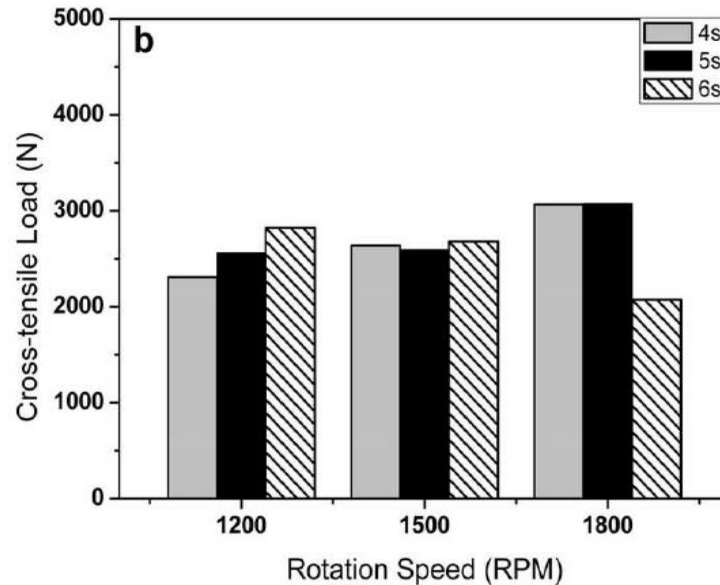


Figure 22: Correlation between cross-tensile load and rotation speed [39]

1.4 Motivation and Objective

For the purpose of joining dissimilar materials especially aluminum, magnesium, and high strength steel with high strength joints, refill friction stir spot welding is employed as a non-melting joining technology with less defects involved. However, there is little literature concerning the metallurgy, mechanical properties, and methods for parameter optimization in RFSSW. This thesis is focused on exploring these aspects. The objective of this thesis is to improve the mechanical performance of friction stir welding. In particular, the tasks of the experiments are as follows:

1. Investigate the microstructure of RFSSW joints of Al 6061 with DP 600 steel, and ZEK100 with DP 600.
2. Optimize the parameters of RFSSW dissimilar joints to achieve the highest strength through observation of microstructure and tensile/shear test results.
3. Explore the bonding mechanism of RFSSW joints through various characterization techniques such as SEM, Electron Diffraction Spectroscopy (EDS), X-ray Diffraction Analysis (XRD), and TEM.

1.5 Thesis layout

This thesis consists of six chapters and appendices. First of all, Chapter one gives a general introduction to FSW and RFSSW techniques, including the application in the industry and advantages over other joining methods. Some of the most representative literature on topics associated with RFSSW of dissimilar alloys are also reviewed. Then Chapter two elaborates on the experimental apparatus and methods used in this research. In Chapter three to Chapter five the microstructure and mechanical properties of the dissimilar RFSSW joints produced in this research are investigated and discussed. Chapter three is focused on dissimilar friction stir seam welding of Al 5754 and DP 600 steel for comparison purposes to RFSSW joints. Chapter four describes the work done on RFSSW of Al 6061 alloy and DP 600 steel. Chapter five elaborates on the results of RFSSW of ZEK 100 and DP 600 steel. Chapter six clarifies key results, conclusions, recommendations of future work, and bonding mechanism behind successful joining of dissimilar alloys by RFSSW.

Chapter 2: Experimental Apparatus and Methods

2.1 Base material studied

Welding sheets used in the Al alloy/Steel FSW study were Al 5754 of 2.2 mm in thickness and DP 600 dual phase steel of 2.5 mm in thickness. Dimensions of the Al alloy welding coupons were 140mm by 30mm with a 30mm overlap area.

Samples were welded with two travel speeds, 16 and 45mm/min, respectively to compare the microstructure and mechanical properties of the welds made by the tool using the two speeds. Temperature measurement was done using a K-type thermocouple taped in the grooves cut on the surface of the steel plate.

Welding sheets used in Al alloy/Steel RFSSW study were Al 6063. Dimensions of the Al alloy welding coupons were 100 mm x 25 mm with 1.3 mm in thickness, and the DP 600 was 1 mm thick with a 10 µm thick hot-dip-galvanized Zn coating.

Ultimate tensile strength (UTS) for the Al 6063 alloy is 241Mpa. The coupons were 100 x 25 mm, with a 25 mm overlap. During welding trials, the DP 600 sheet was maintained on the bottom position, and the plunging depth of the tool into the upper Al 6063 sheet was varied from 1.0 to 1.2 mm.

Welding sheets used in Mg alloy/Steel RFSSW study were commercially available sheets of Mg alloy ZEK 100. Dimensions of the Mg alloy welding coupons were 100 mm x 25 mm with 1.53mm in thickness. The DP 600 was dual phase steel with 600 MPa minimum tensile strength with 1 mm in thickness coated with a 10 µm thick hot-dip-galvanized Zn layer.

The compositions of the sheet materials examined are summarised in Table 1.

Table 1: Base material compositions from chemistry analysis report

	Al	Mg	Fe	Si	Mo	Cr	Cu	Mn	Zn	Nd	Zr	C	Source
Al 606 3	Bal.	0.49	0.2	0.39	<0.0 1	<0.0 1	0.02	0.03	<0.0 1	<0.0 1	<0.0 1	<0.0 1	Matwe b
Al 646 3	Bal.	0.60	0.13	0.48	<0.0 1	0.02	0.07	0.08	<0.0 1	<0.0 1	<0.0 1	<0.0 1	
ZEK 100	<0.0 1	Bal.	<0.0 1	<0.0 1	<0.0 1	<0.0 1	<0.0 1	0.01	1.3	0.2	0.25	<0.0 1	
DP 600	0.05	<0.0 1	Bal.	0.35	0.01	0.02	0.03	1.8	0.01	<0.0 1	<0.0 1	0.09	
Al 575 4	Bal.	3.13	0.17	0.05	<0.0 1	<0.0 1	0.23	<0.0 1	<0.0 1	<0.0 1	<0.0 1	<0.0 1	

The coupons were 100 x 25 mm, with a 25 mm overlap. During welding trials, the DP 600 sheet was maintained on the bottom, and the plunging depth of the tool into the upper ZEK 100 sheet was varied from 1.3 to 1.5 mm. Such precision is readily achieved using the servomechanically controlled motion system, which has a precision of 0.01 mm. However, it should be noted that the welding system does not measure the actual thickness of the sheet, and so if thickness variations in the upper sheet material exceed 0.03 mm, there is a risk of the tool contacting with the lower steel sheet, thus causing wear on the tool sleeve due to the nonuniform surface of the steel.

2.2 Welding equipment

Preliminary tests examined friction stir welding to produce overlap seam joints in Al 5754 and DP600. The equipment used in the project is a displaced manual milling machine friction stir welder (Jafo manual milling machine) (See Fig. 23). It includes a 7.5 HP spindle, which has a tool rotation speed in the range of 56 to 1800 RPM. The travel speed of the welding head is between 11 to 2000 mm/min. This machine is suitable for friction stir welding for aluminum and magnesium alloys of 1 to 12 mm in thickness, and steels less than 2mm.



Figure 23: Friction stir welder (Jafo manual milling machine) [40]

The refill friction stir spot welder employed in this master thesis project is the RPS100 spot FSW system from Harms&Wende in Germany (See Fig. 24) [41]. It contains a three-piece non-consumable tool including an inner pin, outer shoulder, and clamping ring. Every component of the three is mounted on a separate actuation system. A water cooling system is integrated onto the collar surrounding the three-piece tool to remove heat.

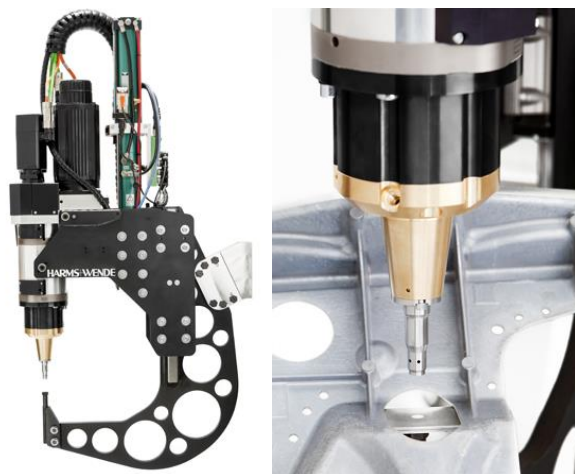


Figure 24: RPS100 spot friction welding system

All production parameters are displayed in the Edit menu shown in Fig. 25. A recipe can be edited with up to ten position points. The position points are moved to sequentially by the machine and determine the welding process.

The screenshot shows a software interface titled 'RPS100 Parameter' with a sub-section '2. Welding parameters'. It contains a table with columns for PKT, Time [sec], Spindle n[1/min], Sleeve Travel[mm], Pin, Sp Interpol., and H. The rows represent different points in the welding process: DR (between welds), 1 (initial friction phase), 2 (depth of sleeve travel), 3 (retract sleeve), and 4 (end of process).

PKT	Time [sec]	Spindle n[1/min]	Sleeve Travel[mm]	Pin	Sp Interpol.	H
DR	0.000	300	0.000	0.000	2	80
1	0.200	2100	0.000	0.000	2	4
2	1.550	2100	1.450	- 1.466	2	4
3	1.400	2100	0.000	0.000	2	80
4	0.000	0	0.000	0.000	0	0

Figure 25: Welding parameters edit menu of refill friction stir spot machine

The top line 'DR' is what speed the tooling will spin at between welds. It applies 300-400 RPM to keep the tools rotating and prevents the accumulated material from clogging the tooling. Line 1 is set as the initial friction phase and used to generate frictional heat into the parts by rotating the tool. Line 2 is used to program the depth the sleeve will travel. The general guide is to travel 0.1-0.2 mm into the bottom sheet if hardness of bottom sheet is lower than tool material. The pin travel will automatically be calculated by the program. The time is based on how far the sleeve has to travel. Line 3 is used to retract the sleeve and produce a flat weld face. The last two columns are Sp and H. According to Harms and Wende, the parameters must be set up exactly the same as those in the picture for all the recipes. They affect how fast the weld head rotate and the tool move up and down.

Welding parameters used in the study are summarised in Table 2.

Table 2: Welding parameters and their range of quantity

Rotation speed(RPM)	1200 - 2100
Plunging depth(mm)	0.3 – 0.1 above the interface
Welding cycle(s)	2.5 – 3.5

This state-of-the-art technique, although creative, has issues with material sticking to the tool surfaces. The sleeve displaces a great amount of material and requires the relatively smaller diameter pin to push a long distance to maintain constant volume exchange. This long retract distance brings the plasticized material at elevated temperature onto a cooler region of the inner wall of the shoulder, where the sticking problem happens. This leads to the pin becoming wedged in the shoulder between weld cycles due to build-up of weld metal. However, a modification to the pin and shoulder relative positioning was suggested. During step 1, the pin is extended past the shoulder to a length that ensures a constant volume exchange between the material stirred by the pin and that pressed upon beneath the shoulder. During step 2, the tool set plunges to a desired depth with a constant plunge rate. The pin is then retracted into the shoulder under position control, while the shoulder extrudes the material back into the void left as the pin is retracted. At the completed retracted position, the shoulder and pin are nominally flush with the sheet surface. At step 4, rotation will stop and a second weld cycle may be employed. The refill FSSW process has been shown to produce high joint strengths with minimal indentation and few internal void defects.

2.3 Mechanical Testing

Three samples of welded specimens per condition were tested through tensile shear testing. An Instron 4206 (Norwood, MA) tensile test machine (see Fig. 26) was used in this study, where specimens were strained to failure with a cross head speed of 1 mm/min. The geometry of the welding coupons for tensile shear test as well as the test set-up are shown on Figure 27.

Alignment spacer sheets were used to grip the samples during overlap shear testing to minimize bending or misalignment effects.

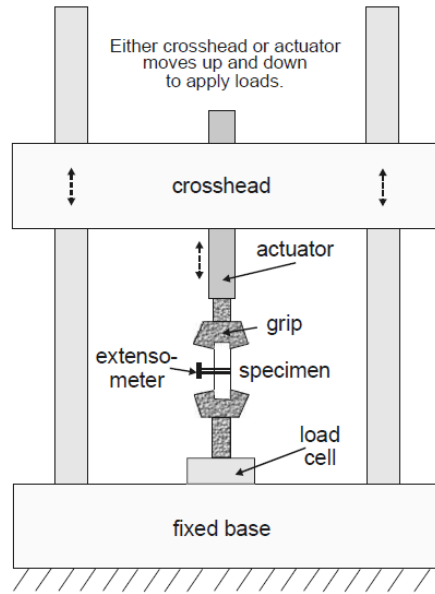


Figure 26: Schematic of Instron 4206 (Norwood, MA) tensile test machine [40]

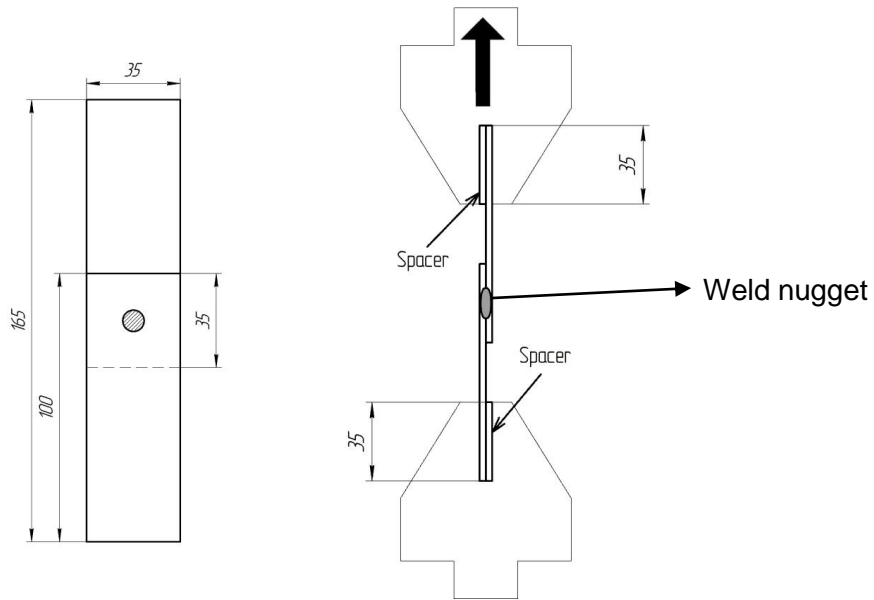


Figure 27: Test coupon geometry and tensile shear test set-up [40]

2.4 Metallographic Analysis

Samples of welded sheets were sectioned, mounted, ground, polished, and etched for a good microstructural observation.

Optical microscopy (OM) was used to determine the size of the stir zone, and scanning electron microscopy (SEM) was used to study the interfacial phases. The ISC (IS Capture) system was used for optical micrographic analysis in this project [39]. SEM microscope used was a JEOL JSM-6460 equipped with Oxford Instruments INCA-350 energy-dispersive spectroscopy system (See Fig. 28) [39]. Transmission electron microscopy (TEM) using a JEOL 2010 model was conducted following extraction of samples using focused ion beam. The specimens were examined using a combination of bright field TEM and high angle annular dark field (HAADF) imaging modes, along with element mapping using EDX [39].



Figure 28: JEOL JSM-6460 equipped with Oxford Instruments INCA-350 energy-dispersive spectroscopy system (left) and JEOL 2010 TEM/STEM is a field emission Transmission Electron Microscope (right) [40]

Acetic-Picric etching solution (acetic acid – 20 mL; picric acid – 3 g; ethanol – 50 mL; water – 20 mL) was used for etching of the Mg alloy while the Al alloy was etched with a mixed two-component chemical solution of: 1mL H₂O/6mL/HNO₃/1mL/HF/12mLHCl, and 25mL HNO₃/1g H₂CrO₄/10mL H₂O for about 5 to 10 sec. 3% nitric acid was used to reveal the microstructure of DP 600 steel. The fracture surfaces of the samples were examined by JEOL JSM-6460 and X-Ray diffraction techniques (XRD) using a Rigaku Ultima IV with a Co K-alpha source after tensile shear testing.

2.5 Microhardness Testing

The Vickers hardness distributions of the welds made at different welding conditions were measured and compared to observe the influence of different parameters on joint properties.

The load was kept at 100g and cycle time for 15s.

Chapter 3: FSW of Al 5754 to DP 600

Joining dissimilar materials is normally more difficult than similar materials with minor difference in composition, since there are a large number of factors that influence the quality of a dissimilar materials joint, such as formation of brittle intermetallic compounds during joining which might cause fracture, need for pre and post heating to minimize stresses during welding and cooling.

In comparison to spot welding, a preliminary study was conducted by using FSW. In this experiment, lap welds were made between Al 5754 and DP 600 steel (aluminum plate top, and steel plate bottom). The effects of welding parameters (i.e. travel speeds and penetration depth into lower steel sheet) on the interfacial bonding, tensile strength, and failure mechanism were investigated. The results show that the intermetallic compound Fe_4Al_{13} was detected at the Al/Fe interface. The weld strength increases significantly by increasing the penetration depth into the lower steel substrate at all travel speeds.

From Fig. 29(a) and Fig. 29(b), it can be revealed that there is a difference of the hook height between welds made under different travel speeds. When the travel speed is lower, the height of the hook is larger so that the mechanical interlock between the upper and lower sheets is stronger than that of hook in the weld made under a quicker travel speed.

As indicated in Fig. 29(c), dynamic recrystallization, as indicated by equiaxed fine grains, occurs in the steel under the Al/Fe interface because the steel undergoes heavy plastic deformation during the FSW process [40]. The SEM micrographs (20kV, X60 and X1000) of the interfacial locations in the weld produced at a speed of 16 mm/min are shown in Fig. 30. The presence of extensive IMCs is detected in both locations on the Al side in Fig. 30 (b). These are thought to be Al rich IMCs.

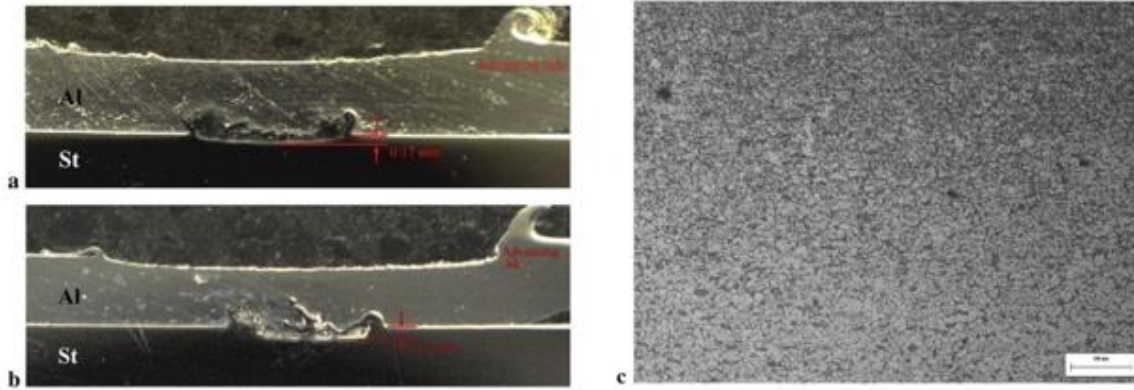


Figure 29: Optical micrographs of Al 5754/DP 600 weld produced at the travel speed of (a) 45 mm/min, and (b) 16 mm/min, (c) microstructure of steel directly under the tip of the pin [40]

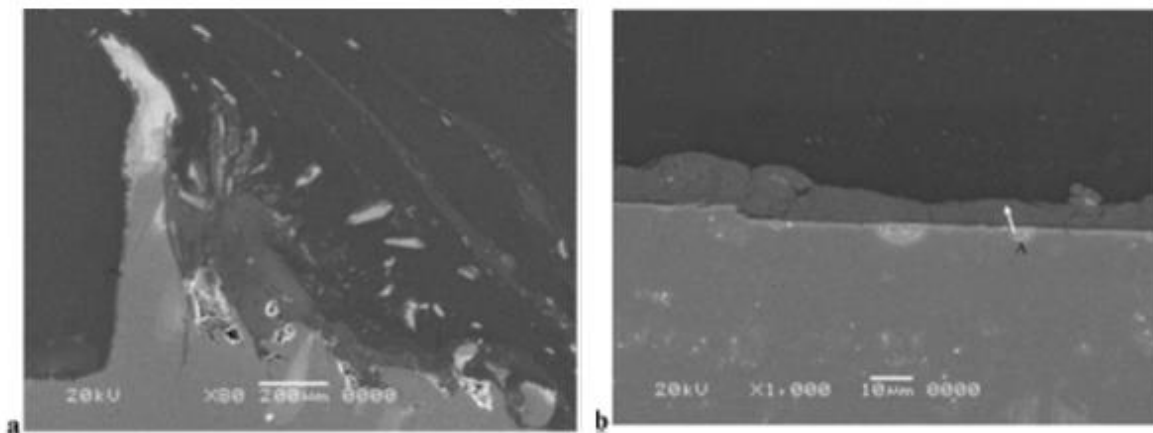


Figure 30: SEM micrograph of interface near the boundary of the stir zone, and (b) Al/Fe interface in the middle of the stir zone [40]

Two travel speeds are used in this experiment, 16 mm/min and 45 mm/min, respectively. The plunging force from the pin into the welding sheets at the lower travel speed tends to be higher in the welding process [41]. The penetration depth vs fracture load curve for welds made at the two travel speeds are shown in Fig. 31. The error bars represent the standard deviation of the results obtained from more than three repetitive tensile testing results for each condition. The results also suggest that the tensile strength decreases and then increases with increasing penetration depth for both travel speeds. A weld with optimized strength can be obtained by maintaining the tip of the pin approximately 0.1 mm above the Al/Fe interface, since this

promotes an interfacial layer with fewer cracks at the Al/Fe interface through an indirect diffusion joining mechanism [13]. The interfacial layer is similar to what has been found by Gendo *et al.* [19], in which diffusion bonding took place via diffusion of the coating layer at the steel surface into the aluminum material from the sheet.

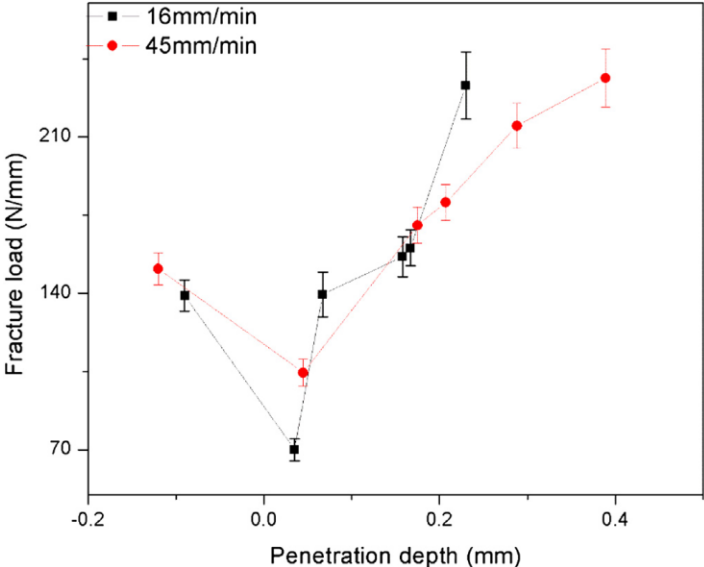


Figure 31: Correlation between fracture load and penetration depth of the pin into the steel [40]

Chapter 4: RFSSW of Al 6063 to DP 600

Considering the few studies on joining of aluminum to steel, the present chapter summarises the results obtained when RFSSW parameters were varied while joining Al 6063 alloy to DP 600 steel. One major issue that was encountered was the poor weldability due the adhesion of aluminum material to the RFSSW tooling. This led to inferior joint properties due to removal of weld metal from the sheet surface, and so the precise tool pin and sleeve displacements were varied in order to identify suitable parameters for welding.

Based on the American Welding Society (AWS) D8.1M:2007 standard [42], the minimum recommended shear tension load for resistance spot welds in aluminum and steel can be calculated from the following equation:

$$ST = \frac{(-6.36E^{-7} \times S^2 + 6.58E^{-4} \times S + 1.674) \times S \times 4 \times t^{1.5}}{1000} \quad (Eq. 1)$$

Where S is the BM shear strength in MPa, and t is the sheet thickness in mm.

In this chapter, this equation is also applied for the case of refill friction stir spot welding, making a comparison between the actual weld strength and calculated minimum recommended shear tension load for friction spot welds.

4.1 Influence of processing parameters on adhesion to the tool

Although prior work demonstrated that RFSSW could be applied to join Al 6181 to DP 600, there was no indication given that weld metal could adhere to the tool surface. In the present work, when a range of parameters was applied to joining Al 6063 and DP 600 steel, a major issue was encountered due to the adhesion of stir zone material to RFSSW tool. This led to a partial removal of the stir zone as shown in Fig. 32, leaving negligible bonded area between the sheets and a large gouge on the sheet surface. Before carrying out further welding, this adhered material needed to be manually removed from the tooling, which was rather time consuming. The welds shown in Fig. 32 were produce using parameters which ranged from 1500 to 2100RPM. Only one successful weld was completed, using a plunge depth of 0.3 mm, which provided an overlap strength of 0.4 kN, far below the AWS recommended requirement of 1.5 kN, based on the upper sheet strength and thickness. After closer examination, it appears the Al

6063 material adheres due to mechanical forging onto the tool surface, since it is readily chiselled off, suggesting it is not metallurgically bonded to the tool.

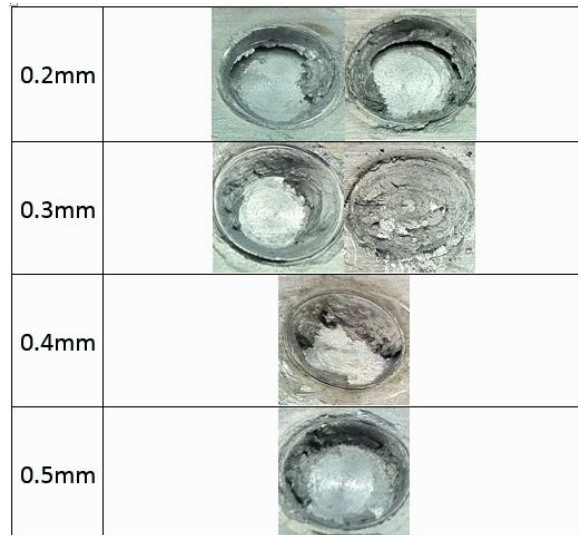


Figure 32: Weld surface in RFSSW joints between Al 6063 and DP 600, produce using 1800RPM, 2.5s welding time and various plunge depths

The feasibility of joining these two dissimilar materials was then evaluated further by adjusting the rate of pin and sleeve movement during welding. This provided more time for material to flow into the pin cavity during welding, and return to the weld as the material is forged by the pin during the retract stage. It was found that retraction time could be varied control the surface quality and tendency for aluminum to adhere to the tool (see table 3 for welding parameters). It was concluded that the weld surface was ideal when the tool retract time increased from 0.5 to 1.5 s. A good quality weld is shown in Fig. 33.

Table 3: Detailed parameters and tool travel speeds during Al 6063/DP 600 welding

RFSSW phases	Time/s	Rotation speed/RPM	Plunging depth of sleeve/mm	Corresponded retract depth of pin/mm
DR	0	500	0	0
Dwell	0.5	1800	0.1	0.1
Plunge	1.5	1800	1.3	1.1
Retract	0.5/1.0/1.5	1800	0	0



Figure 33: Weld surface of refill friction stir spot weld of Al 6063/DP 600 under the condition of 1800rpm, 2s of dwell time, 1.1mm of plunge depth, 1.5s of retract time

The optical micrographs are shown in Fig. 34 for the Al 6063/DP 600 RFSSW joint produced using 2100 RPM, a 1.1 mm plunge depth and 3.5 s welding time (2s of dwell time and 1.5s of retract time). The joints exhibited continuous bonding at the interface, however some voids formed in the aluminum stir zone, as noted by the black region. Following etching, a dark region was revealed at the periphery of the weld in the location which would correspond to the location below the tool sleeve.

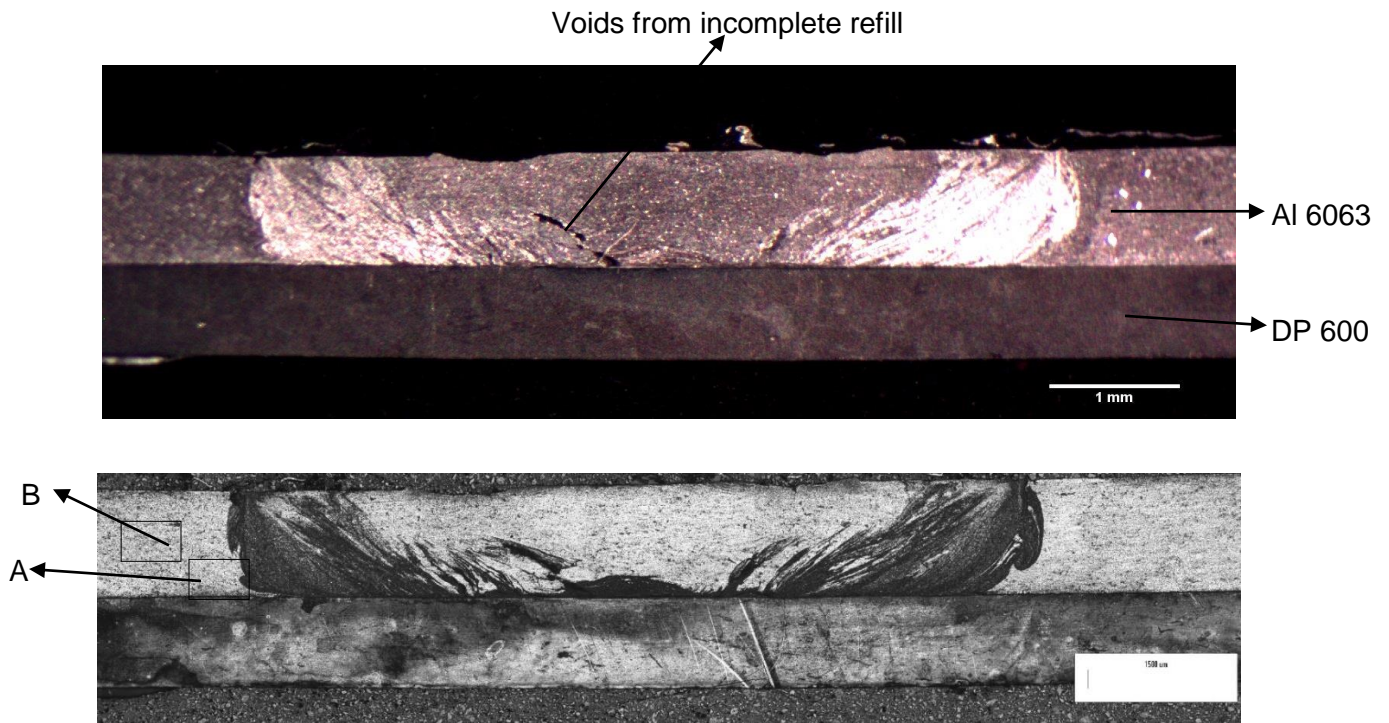


Figure 34: Optical micrographs of RFSSW joint between Al 6063/DP 600 using (a) stereo microscope using indirect lighting and (b) compound metallographic microscope using incident light

In order to understand the microstructure of the dark region, Energy-dispersive X-ray spectroscopy (EDX) was performed on the dark region, specifically across the interface between Al 6063 and DP 600. Fig. 35 and Fig. 36 show the element mapping and line scan results, respectively. From the mapping result, it can be seen that a continuous layer of zinc is covered on the surface of DP 600.

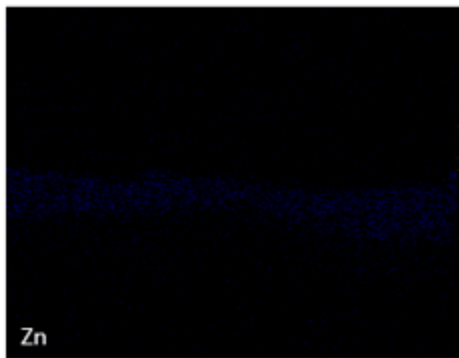
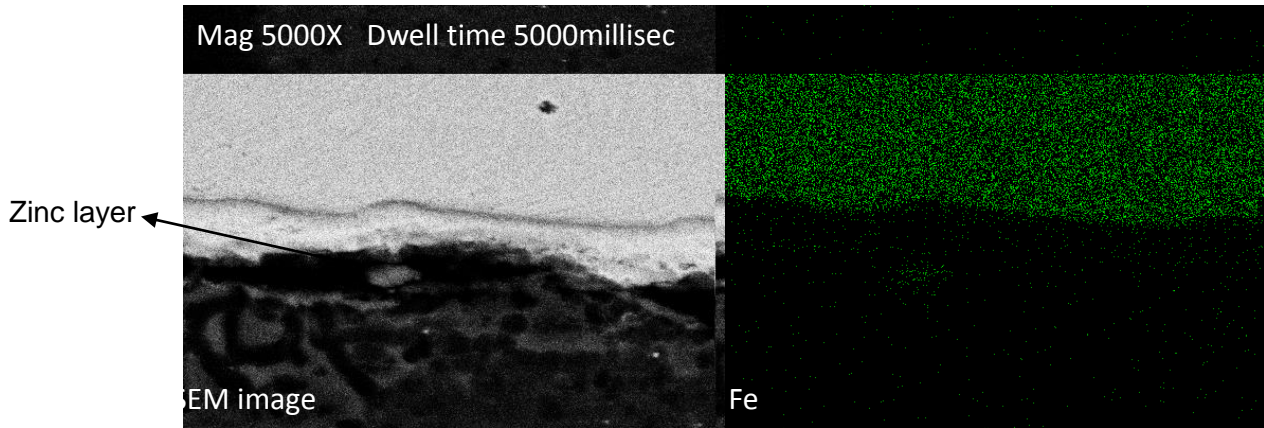


Figure 35: Steel coating layer EDX mapping analysis

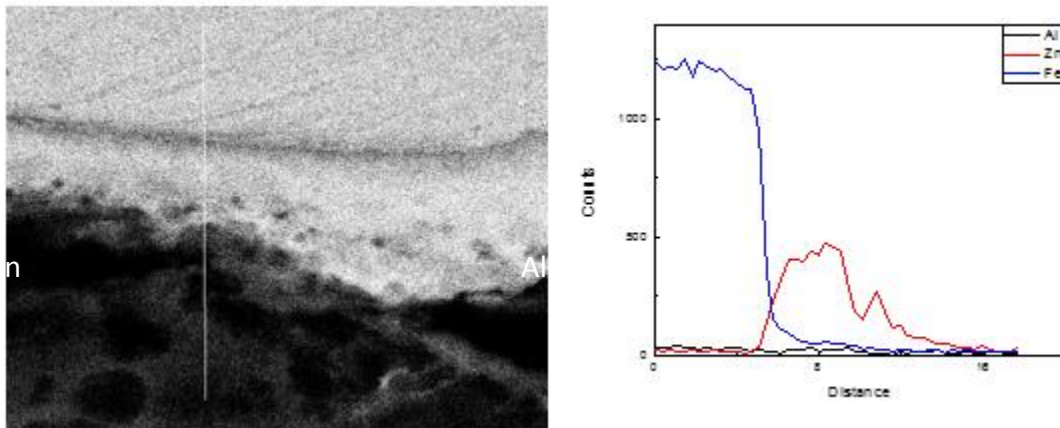


Figure 36: DP 600 coating layer EDX line analysis

As the zinc layer is confirmed through EDX results, it can be concluded that the dark region was formed by accelerated etching, which was motivated by the presence of displaced zinc, which

originated from the zinc galvanized coating on the DP 600 surface. This zinc was stirred away from the surface by the tool and dispersed into the upper sheet of Al 6063 as part of the material flow produced in the stir zone.

At a higher magnification of X100, the refinement of the grain size around the sleeve region in the aluminum sheet was clearly revealed. Fig. 37 shows regions in the outer periphery of the weld near the sheet interfaces. This indicates the material that flows around the sleeve undergoes extreme plastic transformation, contributing to a recrystallization of the aluminum and promotes an equiaxed refined grain size in zone A from Fig. 34. In zone B, there is much coarser grains than those in zone A.

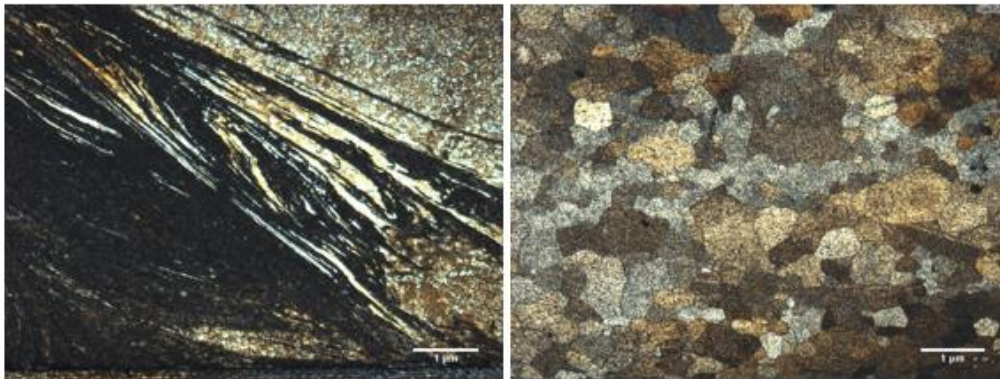


Figure 37: Refined microstructure at the periphery of the stir zone from area A (left) and coarse grains in the heat affected zone from area B (right)

The scanning electron micrographs (20kV, 1000X and 10000X) near the periphery of the bonded region in an Al 6063/DP 600 joint are shown in Fig. 38. A small void was noted at the outer boundary of the joint interface, and the surface of the steel has been deformed by the force of the sleeve during welding. The formation of voids in RFSSW joints has been noted as a result of possible incomplete refilling and lack of material flow [26]. The most striking feature of this microstructure is the fact that no intermetallic compounds were evident at the interface, as shown in Fig. 38(b). It is certainly possible that some intermetallic compounds have formed at a finer scale, however these may have a thickness well under 1 µm since these could not be resolved by SEM. The other striking feature is that the Zn coating on the DP 600 steel has been completely displaced, and Zn could not be detected at the interface in the micrographs shown in Fig. 38.

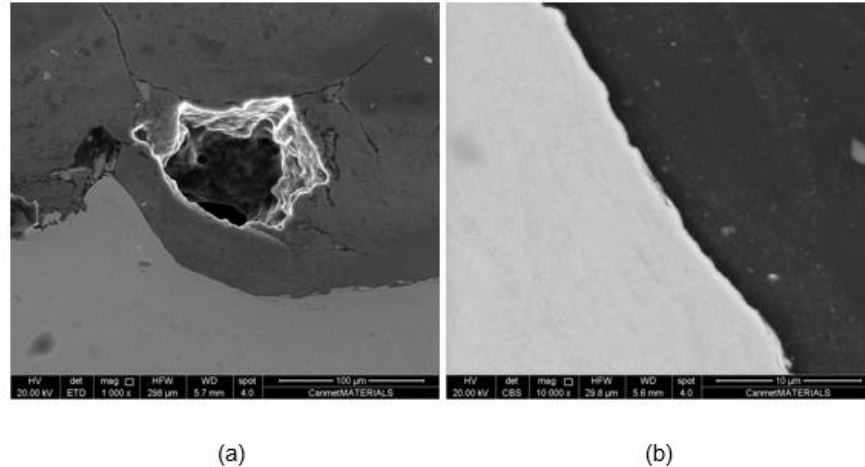


Figure 38: (a) Outer periphery of Al 6063/DP 600 joint bonded region, and (b) high magnification image of the Al 6063/DP 600 interface

4.2 Mechanical Properties

Since it was possible to produce a sound weld after extending the retract time to 1.5s, the mechanical properties of the joints were then evaluated. The highest overlap fracture load achieved in Al 6063/DP 600 joints was 3.7 kN when using a tool speed of 2100 RPM, plunge depth of 1.1 mm, and a welding time of 3.5 seconds. As a further comparison, the fracture loads under different conditions were measured up to three repetitive times shown in Fig. 39(left) with stand deviation as the error bar. When the fracture load is divided by the observed bonded areas, the apparent fracture shear stress may be estimated. This is calculated for comparison to the fracture loads in Fig. 39(right), and reveals a similar trend to the fracture loads with a maximum apparent shear fracture stress of 110 MPa. This is a result of the bonded areas being all similar for each of the conditions, and suggest that the shear stress may be approximately 46% of the tensile stress of the Al 6063 base material. The dip might be from a potential defect due to excessive heating under the condition of 1800rpm, 3.5s.

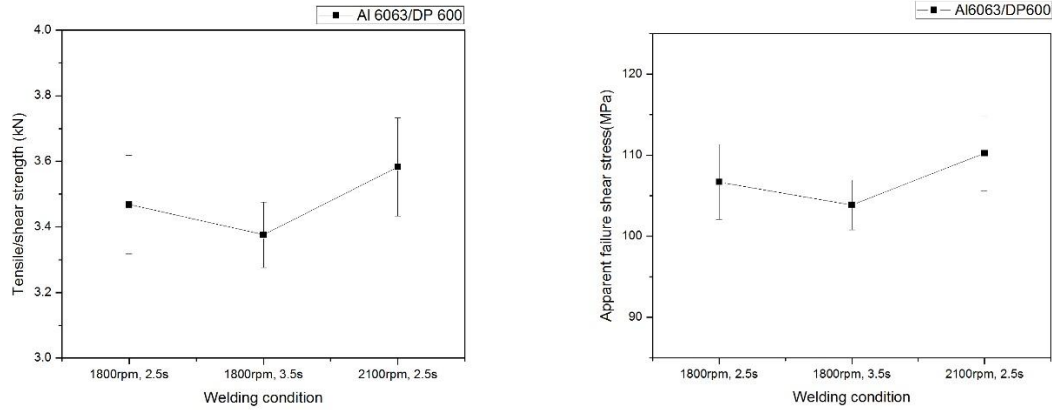


Figure 39: Tensile/shear results of Al 6063 and DP 600 at various welding conditions with the plunging depth uniform at 1.1mm

4.3 Summary

Overall, the tensile/shear testing results show that bonding between Al 6063 and DP 600 is possible using RFSSW. Material adhesion was encountered when the tool retract speeds were too short, and this was solved by increasing the retract time to 1.5 seconds in order to allow plasticized material to detach from the tool surface before the tool is completely retracted. The zinc layer on the surface of the DP 600 was completely stirred away and distributed throughout the upper sheet, which may help to promote bonding between the two sheets. The tool rotational speed played the most significant role in the joint mechanical performance.

Chapter 5: RFSSW of ZEK 100 to DP 600

Joining of ZEK 100 Mg alloy and Zn coated DP 600 steel sheets was studied using RFSSW. The RFSSW process involves a tool with independently moving sleeve and pin components, which rotate at a constant speed and penetrate into only the top sheet. Welds between these two sheets could be achieved, which exceeded 4.7 kN shear strength, using the following process parameters: 1800 RPM tool speed, 3.0 s welding time and 1.5 mm of penetration into the upper ZEK 100 sheet. Scanning electron (SEM) and TEM are used to characterize the Mg/steel interface. It is revealed that a continuous layer of FeAl_2 particles accommodate bonding of the sheets, which appears to have originated from the galvanized coating on the DP 600.

A tool composed of high temperature tool steel with an outer shoulder diameter of 10 mm, and a pin diameter of 6.3 mm was used in all tests, with a rotation speed of 1600 to 2100 RPM and a welding time of 2.5-3.5 s. After welding, spot welds were sectioned and prepared for metallographic examination using standard techniques with final polishing being conducted with 1 mm diamond abrasive in an oil based suspension to avoid corrosion during polishing, and then etched with picric acid. Optical microscopy was used to determine the size of the stir zone,

And SEM was used to study the interfacial phases. TEM was conducted following extraction of samples using focused ion beam. The specimens were examined using a combination of bright field TEM and HAADF imaging modes, along with element mapping using EDX.

Vickers microhardness testing was conducted using a 200 g load, with a 5 s dwell time. Overlap tensile shear tests were conducted to determine the fracture load and failure mode of the RFSSW specimens. XRD was also conducted on the fracture surfaces following overlap shear testing using a Rigaku Ultima IV diffractometer.

5.1 Interfacial Microstructure Investigation

The weldability of ZEK 100 Mg alloy to DP 600 steel was found to be better than the aluminum alloy combinations examined here. The joint surface appearance and optical microstructure is shown in Fig. 40 for a typical ZEK 100/DP 600 weld. The adhesion of the Mg alloy to the steel tooling was not an issue. The weld surface appeared to be particularly shiny, with a faint mark imposed by the clamping ring as shown in Fig. 40(a). The joint surface appearance and optical

microstructures are shown in Fig. 40(b-d) for each set of welding parameters studied, and bonded diameters of joints varied from 6 to 9 mm.

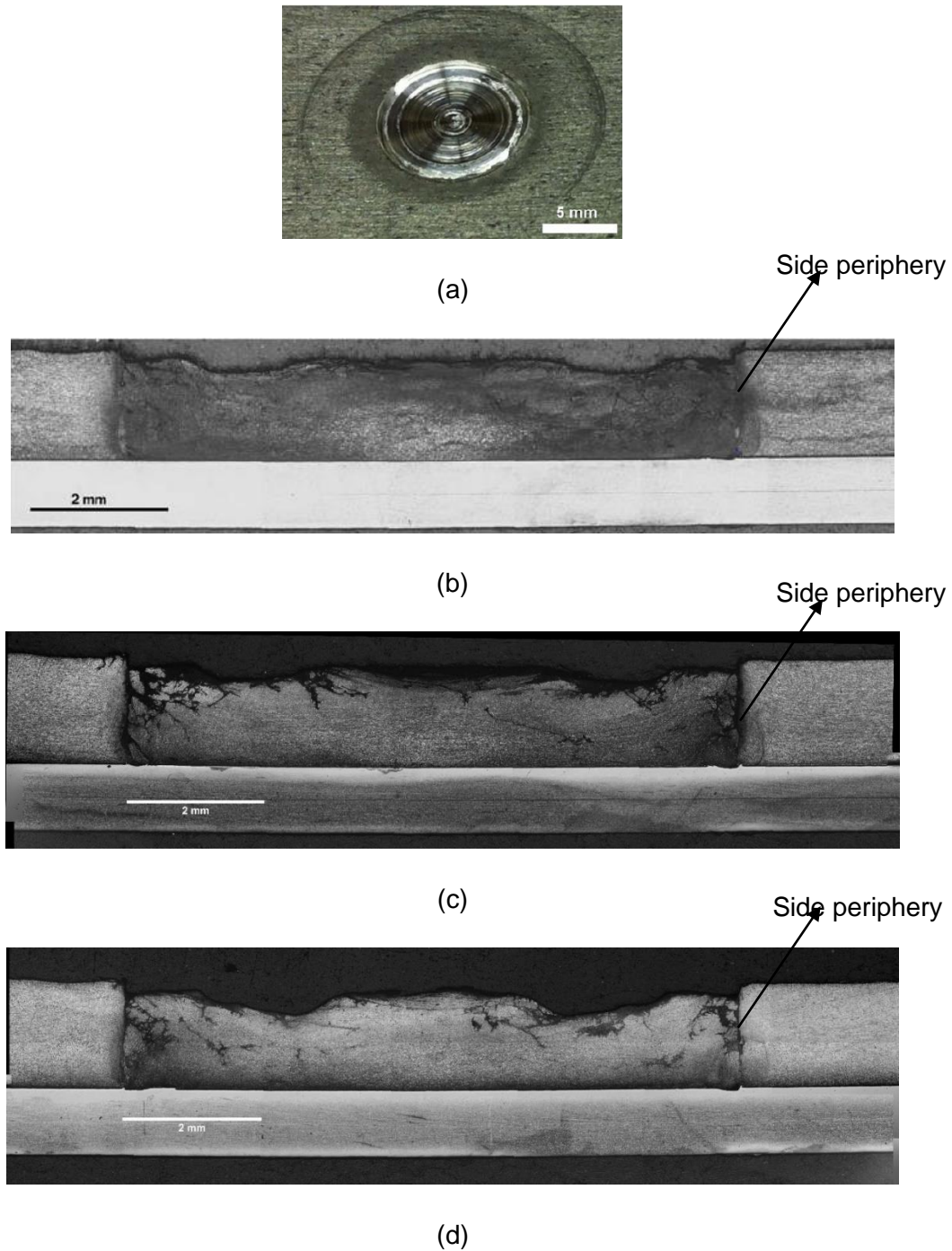


Figure 40: (a) weld surface appearance of ZEK 100/DP 600 joint and (b–d) optical micrograph of ZEK 100/DP 600 joint showing heavily deformed stir zone and bonded interface at condition of 1800 RPM/3 s, 1800 RPM/3.5 s and 2100 RPM/3 s

The stir zone consisted of heavily deformed grains in all of these figures, while the side periphery of the stir zone appeared to etch more aggressively, as noted by the darker appearance in heating may have occurred using these parameters, and it is clear from the micrographs that the surface profile of the welds were nonuniform under these conditions. Owing to the severe mechanical deformation imposed by the tool during the refill process, significant grain refinement occurred in the weld nugget within the side peripheries within the ZEK 100 Mg alloy.

However, since the tool does not penetrate into the steel, no significant microstructural changes were observed in the lower (steel) sheet. The grain size in the ZEK 100 Mg alloy was measured using the linear intercept method and found to range from 1.6 to 6.5 microns in the stir zone, compared to 10 mm in the base material. The variation in grain size was symmetrical across the stir zone, with finer sizes observed towards the location below the tool sleeve at the outer periphery, while the coarser grains were observed near the centreline of the tool below the pin (see Fig. 41). This observation suggests that the strain rates were highest below the tool sleeve, while lower strain rates would be consistent with the location below the pin since the tangential shear rate would approach zero.

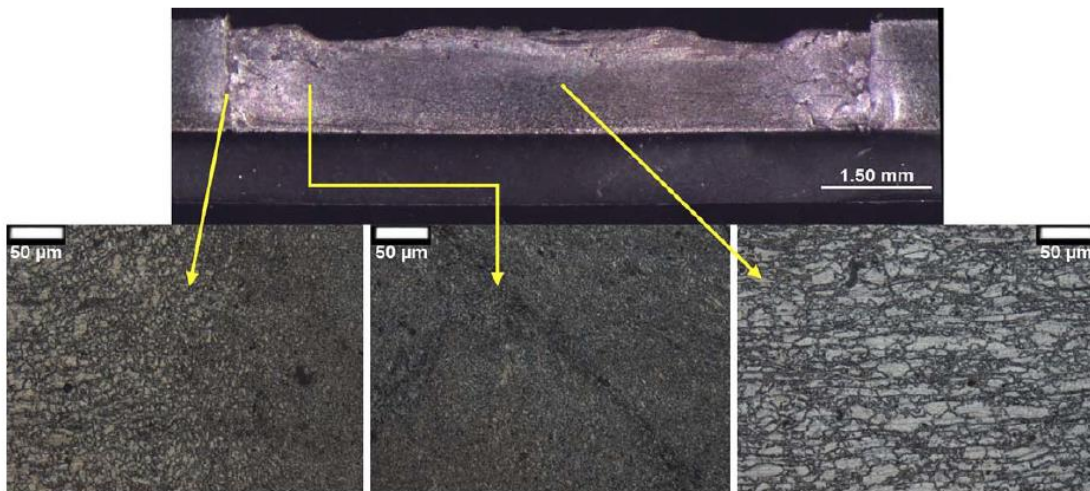
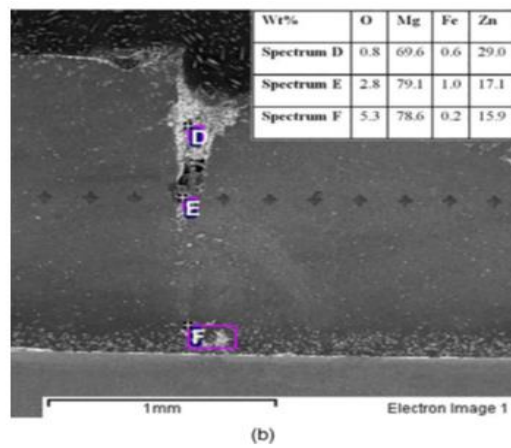
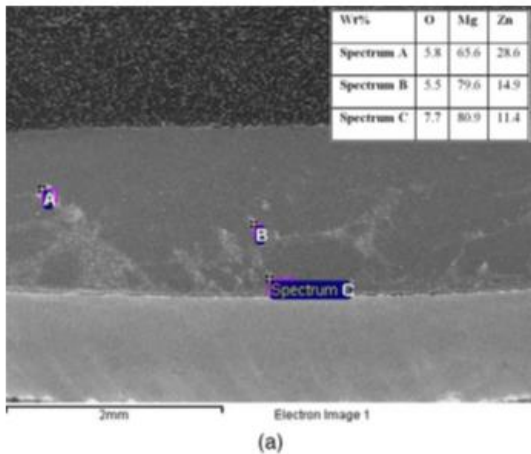


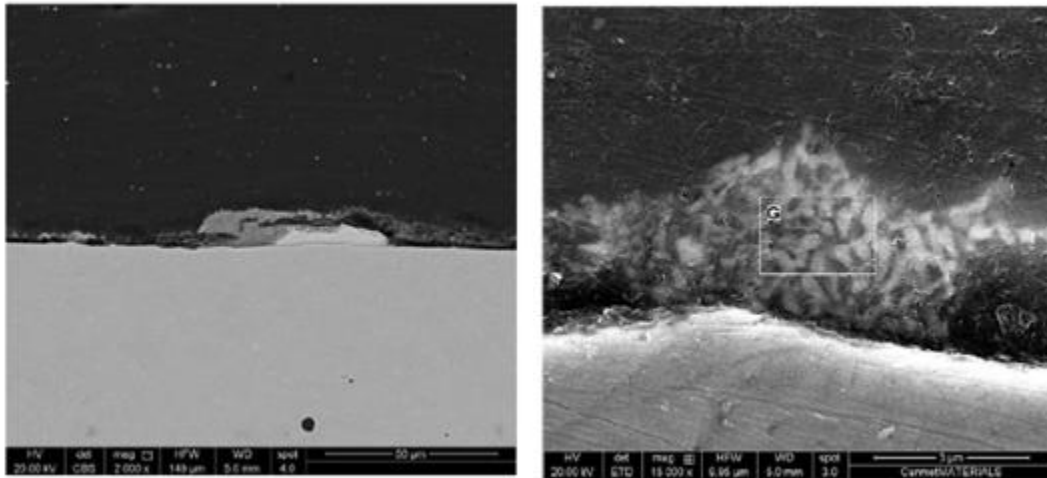
Figure 41: Grain structures in ZEK 100 stir zone produced using 1800 RPM and 3 s

When the microstructures were examined by SEM, it was noted that high concentrations of Zn are dispersed throughout the stir zone in chaotic flow patterns as shown by the light regions in Fig. 42(a). The chemical compositions of locations A–C in the figure were quantified using EDX;

the Zn content ranged from 11.4 to 28.6%. In addition, at the periphery of the joint directly under the tool sleeve, the Zn content ranged from 15.9 to 29.0% as indicated in Fig. 42(b). The Zn coating appears to be displaced from the DP 600 sheet surface and moved upwards as well as towards the periphery edges of the weld; such movement is consistent with the material flow. The welding process involves plunging the tool sleeve first (while the pin retracts), and then the material from the centre of the weld is pushed towards the outer regions by the pin when the refill stage occurs. Owing to the constraint of the surrounding clamp, the material is extruded by the sleeve towards the cavity formed by the pin during the plunging phase. The material is then extruded back into the sheet by the pin during the withdraw phase, which has been modelled numerical in prior work and found to be consistent with interrupted partially welded specimens [42]. As the pin extrudes material from the centre towards the outer boundary of the weld, it will displace the material from the interface towards the surrounding sleeve region [26].

There was evidence that some residual Zn coating on the steel sheet surface remained at the interface of the weld and was not completely displaced by the material flow imposed by the refill welding tool. Examining the interface of the ZEK 100/DP 600 joints in more detail, it can be noted that some residual Zn remains (see Fig. 45(c)).





(c)

(d)

Figure 42: Images (SEM) of ZEK 100/DP 600 joint

Using backscattered electron contrast, it is apparent that some of the Zn has also reacted with the Mg alloy and appears to form a very fine scale Mg–Zn eutectic structure, as indicated by the EDX analysis of area G in Fig. 42(d), which indicated a composition of 54.8Mg–39.3Zn–5.9Fe. This composition and the presence of a eutectic structure is also consistent with interface features

Observed by Schneider et al. when studying magnesium/ steel FSW joints [43]. Considering that the Mg–Fe binary phase diagram indicates that these elements are immiscible even at elevated temperatures, joining of ZEK 100 Mg alloy and DP 600 steel is rather challenging. However, the presence of a Zn coating on the steel appears to provide a mechanism for bonding. Prior work by Gendo et al. showed that strengths in friction stir spot welded Al alloy to steel joints could be considerably improved by modifying the composition of the coating material and selecting alloys with as low a melting point as possible [19]. In order to further investigate the bonding mechanism for joining the Mg alloy and steel sheets, the interfacial region near the centre of the joint was extracted using focused ion beam, and analysed using TEM.

A TEM image of the interface at the centre of the weld is shown in Fig. 43, along with element mapping. In the HAADF image, it can be noted that no voids or pores were present at the interface; however, a discontinuous film of oxides could be observed, which likely originated from the original Mg alloy sheet since the surfaces were not brush finished before joining (as

expected for a manufacturing scenario). The presence of Zn is only observed in the Mg alloy side, with an increased concentration within 250 nm of the steel interface. However, the most striking observation is the presence of an Al rich film with a thickness of ~100 nm at the interface within the Mg alloy sheet.

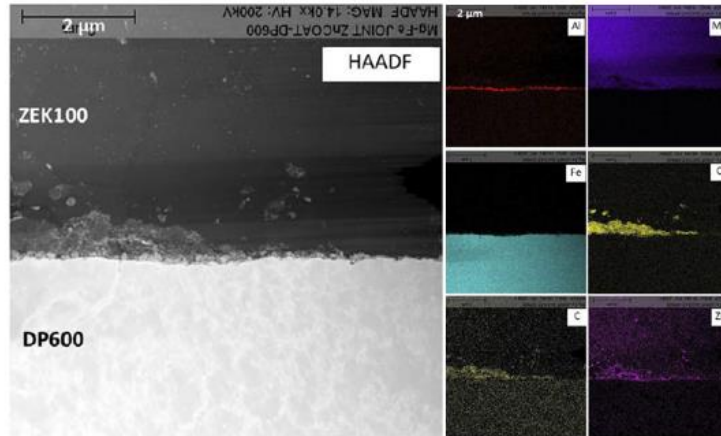


Figure 43: HAADF image (TEM) of interface with element maps for Al, Mg, Fe, O, C and Zn

Fig. 44 shows the HAADF image of the interface at higher magnification, where the Al rich interfacial layer can be more clearly observed to coincide with an intermediate concentration of Fe slightly away from the bulk of the steel. The Al rich film appears to exclude other elements; however, a small increase in the carbon concentration is noted near the interface, which may indicate remnants of contamination on the sheet surfaces that were trapped at the interface. Discontinuous films of oxide and Zn coating are again observed in the O and Zn maps.

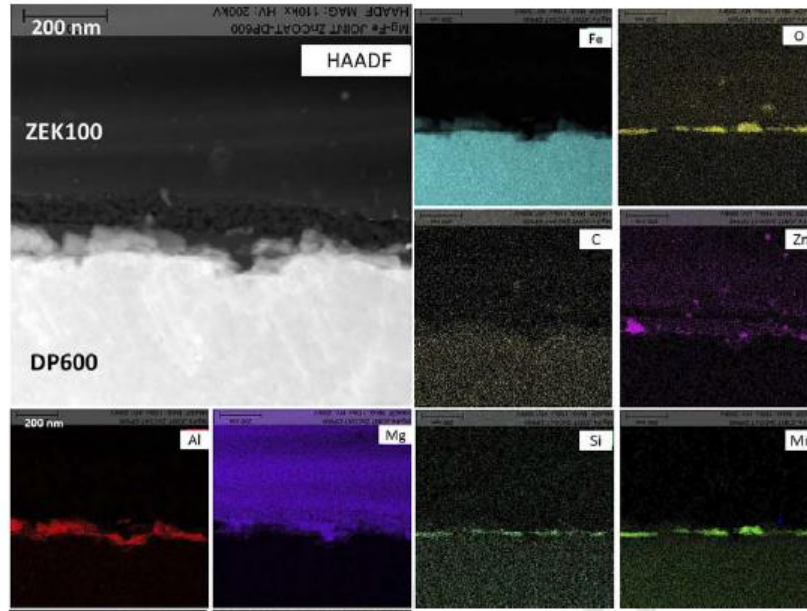


Figure 44: High angular annular dark field image (TEM) of interface with element maps for Al, Mg, Fe, O, C, Zn, Si and Mn

In the bright field TEM image in Fig. 45, the particles rich in Al and Fe can be observed in more detail. These particles averaged in size ~ 50 nm and were embedded well within the Mg phase in the ZEK 100 alloy. These particles were too fine to perform selected area diffraction, and so convergent beam electron diffraction was performed on one of the Al and Fe rich particles indicated by the yellow arrow in Fig. 45. The pattern was indexed as a (110) zone axis, with a lattice parameter that would be consistent with FeAl_2 based on available literature [44]. These findings are rather striking, considering that there is no significant aluminum content in the bulk ZEK 100 and DP 600 alloys. However, it should be noted that, during the continuous hot dip galvanizing process, the DP 600 sheet is dipped in molten zinc, which contains typically 0.15–0.19%Al in order to promote better adhesion and reduce embrittlement of the coating, and this typically forms an Al rich layer at the interface of the Zn coating and steel [45-46]. This explains the origin of the FeAl_2 particles at the interface of the ZEK 100 and DP 600 joints, and these particles appear to serve as an intermediate layer between the Mg alloy and steel grains at the interface.

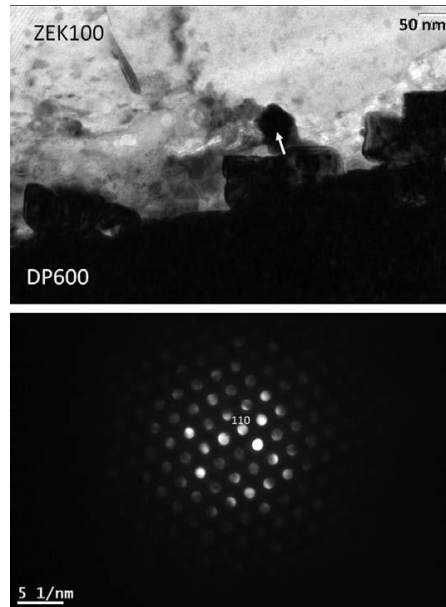


Figure 45: Bright field image (TEM) and corresponding convergent beam electron diffraction pattern of second phase FeAl₂ particle (noted by arrow) observed directly at the ZEK100/ DP600 interface

Following overlap shear testing, the fracture surfaces were analysed to identify possible intermetallics at the interface, since all joints failed along this line. The XRD spectrum shown in Fig. 46 indicates mainly magnesium and iron grains; however, two peaks were identified for FeAl₂. This result is consistent with the TEM observations in Figs. 44 and 45, which suggest that a nanoscale trail of this phase is present across the interface. Evidence of partial bonding was noted around the outer periphery of the stir zone, in the form of a change in the surface morphology of the zinc. A similar feature was noted in the partially melted and brazed surfaces in dissimilar Al/steel and Mg/steel interfaces in the periphery of resistance spot welded dissimilar welds in a prior work [47]. It should also be noted that this change in the coating appearance could be noted around the main fracture area following testing and suggests that temperatures may have been sufficient to melt this coating (at ~419 ° C). The interface temperature measurements reported for similar processing parameters in Al and Mg based alloys and temperature measurements in Al 7075 refill friction stir spot welds that indicated the interface easily exceeds 446 °C [37]. These results suggest that the maximum peak temperatures feasible during RFSSW are likely approaching the melting point of the ZEK100 material. These temperatures would easily facilitate diffusion bonding or brazing of the Zn coating around the outer boundary of the stir zone. Such a brazing effect has also been found to

promote higher joint strengths in conventional FSSW and in resistance spot welding of dissimilar Al/Mg joints utilising Zn coated steel interlayers [47].

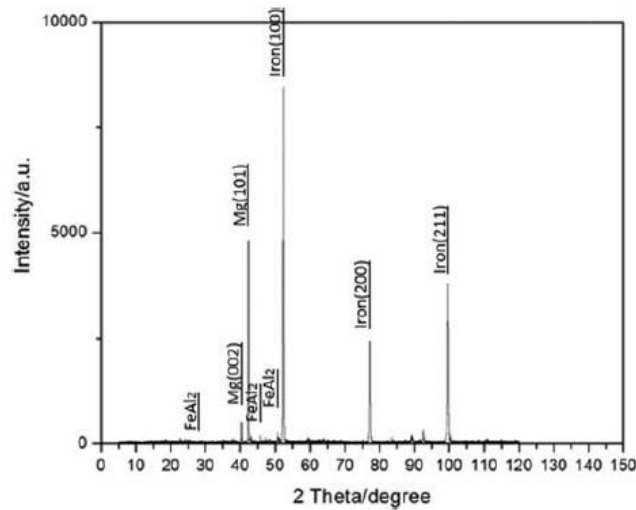


Figure 46: X-ray diffraction pattern of overlap shear fracture surface on steel side

5.2 Microhardness testing

The fine grained structure within the ZEK 100 stir zone resulted in a hardness increase from ~60 HV in the base material, to ~80 HV in the stir zone (Fig. 47). There was also a slight decrease in microhardness at the centreline of the stir zone, and this correlated well with slightly coarser grain sizes, as indicated in Fig. 47(left). This may be explained by the reduced tangential shear strain rates near the centre of the rotating tool, and slower cooling rates to be expected at the centre of the weld. These two factors would produce a coarser recrystallized grain size during deformation, as well as a coarser grain structure with more extensive recovery upon cooling, thus leading to the lower hardness around the centreline.

In contrast, the regions near the outer boundary of the stir zone (3 to 4mm of the distance to the weld centre) shown in Fig. 47 exhibited the finest grains structures, likely due to the higher strain rates imposed by the outer rotating sleeve of the tool, resulting in slightly higher hardness values around this location.

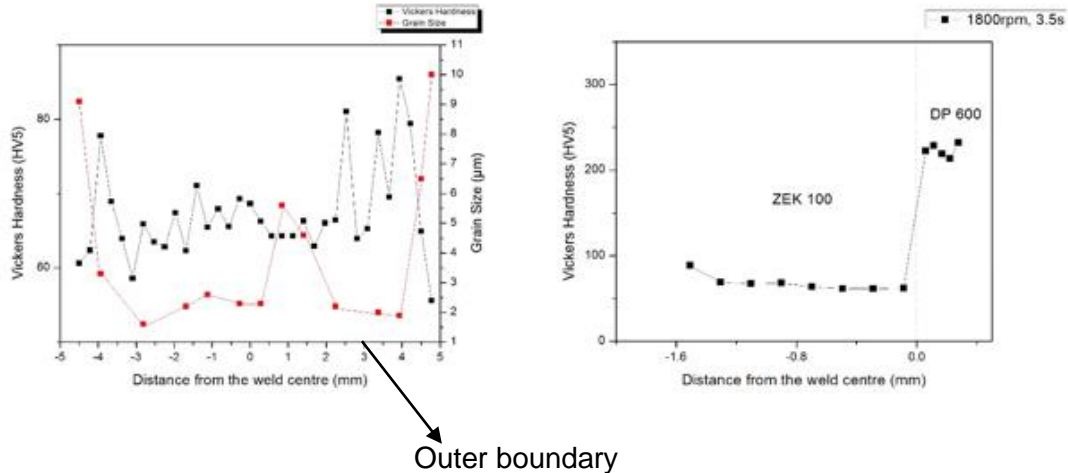


Figure 47: Microhardness profiles a across Mg alloy stir zone in ZEK 100/DP 600 joint when using parameters of 1800 RPM/3.5 s(Left) and along centreline of nugget traverse to interface at condition of 1800 RPM/3.5 s(Right)

5.3 Mechanical Properties

5.3.1 Tensile/shear Results of ZEK 100/DP 600 RFSSW Joints

The overlap shear strengths of individual joints reached over 4.9 kN for the ZEK 100/DP 600 joints; however, as shown in Fig. 48 the highest average load was 4.7 kN when using 1800 RPM, a 3 s welding time and 1.5 mm of tool penetration. This compares well with the requirements of AWS D8.9M [41], which recommends an average of 3.8 kN for the equivalent resistance spot welds between the weaker materials (ZEK 100, which had a tensile strength of 275 MPa). The fracture loads heavily increased when the plunge depth increased above 1.3 mm, which indicates that a critical threshold distance between the tool and steel sheet must be reached in order to provide bonding. When the welding time increased to 3.5 s using 1800RPM, the loads decreased, to an average of 3.45 kN, and when the tool rotation speed increased to 2100RPM, the average fracture load decreased to 3.29 kN. These results suggest that the quality of the bond deteriorates when excess heat is applied during welding. All the fractures during overlap shear testing occurred through the interface.

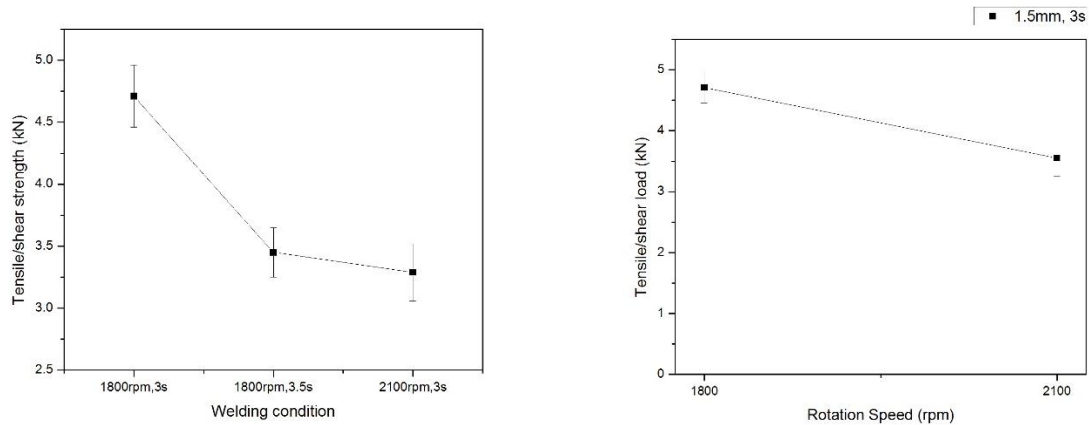


Figure 48: Tensile/shear results of ZEK 100 and DP 600 at various welding conditions with the plunging depth uniform at 1.5mm(Left); Tensile/shear results of ZEK 100 and DP 600 at various plunge depths when the tool speed is 1800RPM and welding time is 3 s(Right)

Fig. 49 shows the displacement curve obtained from the fracture tensile testing of the weld made under the condition of 1800 RPM, 3.5s, and 1.5mm of the plunge depth. The absorbed energy U of the weld under the tensile testing up to the fracture point is the area under the displacement curve. It should be noted that the absorbed energy represents the anti-fracture ability. The higher the absorbed energy it takes before the fracture point, the harder for this material to fracture. In the automobile industry, higher absorbed energy of the car body material also refers to higher durability and higher bearing ability against force upon the material when it comes to crash. U was obtained from the numerical integration of the tensile testing displacement curve by Origin 8, which was calculated to be 2.73 N·m, that is, 2.73 J. As the failure mode is interfacial failure for this weld, the toughness equals to the absorbed energy per unit size. Based on the weld area, the toughness of the weld was calculated to be 11.23J/m³.

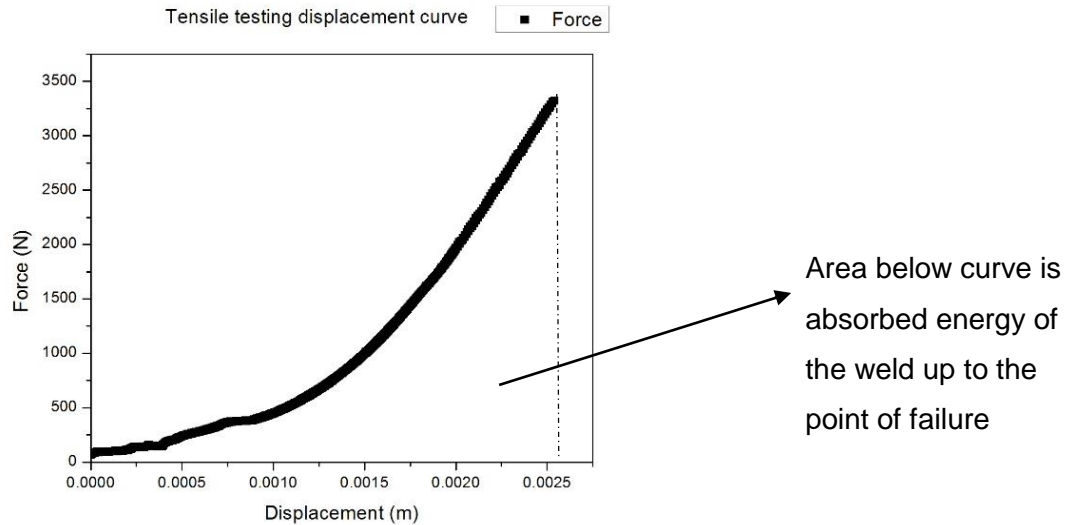


Figure 49: Tensile testing displacement curve of the weld made under the condition of 1800RPM, 3.5s, and 1.5mm of the plunge depth

5.3.2 Comparison of RFSSW of ZEK 100 to DP 600 with/out Zn coating and brush finished ZEK 100 to DP 600 with Zn Coating

In order to investigate the effect of coating on the surface of DP 600 and ZEK 100 on the mechanical properties of the refill friction stir spot joints between ZEK 100 and DP 600, the surface of ZEK 100 and DP 600 was ground with sandpaper in the order of sand particle sizes ranging from 300 grit to 1200 grit. After that, refill friction stir spot joints were made between ZEK 100 and brush finished DP 600, and brush finished ZEK 100 and DP 600. Mechanical testing was done on the joints made. From the results of tensile/shear testing(see Fig. 50), it can be seen that shear strength drops when the coating is removed from the surface of DP 600, while there is no obvious effect on the mechanical properties when the coating on ZEK 100 is removed. As has been discussed before, zinc coating on DP 600 does facilitate the bonding between two dissimilar materials in refill friction stir spot welding.

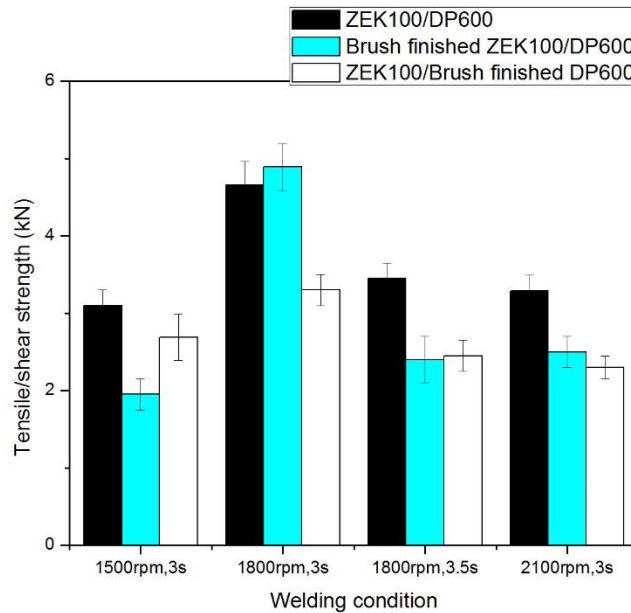


Figure 50: Comparison of tensile/shear load between ZEK 100/DP 600, brush finished ZEK 100/DP 600, and ZEK 100/brush finished DP 600

5.4 Summary

The successful use of RFSSW has been demonstrated for joining ZEK 100 Mg alloy to DP 600 steel sheets. The highest joint strengths in ZEK 100/DP 600 joints averaged 4.7 kN when using parameters of 1800 RPM, a 3.0 s welding time and 1.5 mm of penetration into the upper ZEK 100 sheet. The typical range for bonded diameters of refill friction stir spot welds is varied from 6 to 9 mm. Transmission electron microscopy revealed that the interface is actually decorated with $FeAl_2$, which accommodates bonding between the insoluble Mg and Fe based grain structures in the sheets, and this appears to have originated from the Zn based galvanized coating on the steel. This phase was also confirmed using XRD along the fracture surfaces of overlap shear samples. Zinc coating on DP 600 has a positive effect on the bonding strength of refill friction stir spot joints.

Chapter 6: Conclusions

6.1 General conclusion of dissimilar materials by RFSSW results

Refill friction stir spot welding is feasible in terms of joining dissimilar materials between ZEK 100 magnesium alloys, Al 6063, and DP 600. The bonding mechanism between ZEK 100 and DP 600 has been shown by SEM, EDX, and XRD to be the result of formed IMCs, especially FeAl₂ detected by TEM technique. This appears to have originated from the Zn based galvanized coating on the DP 600, so the zinc coating on DP 600 facilitate the bonding between dissimilar materials.

6.2 Comparison of different materials RFSSW results

Al 6063 has a successful bonding with DP 600 through refill friction stir spot welding with the highest welding strength reaching 3.7kN. There is a key difference of mechanical properties between ZEK 100 RFSSW joints with DP 600 under the same welding condition. The highest joint strengths in ZEK 100/DP 600 joints averaged 4.7 kN when using parameters of 1800 RPM, a 3.0 s welding time and 1.5 mm of penetration into the upper ZEK 100 sheet, which fully met the requirements of AWS D8.9M, which recommends an average of 3.8 kN for the equivalent resistance spot welds between the weaker material (ZEK 100, which had a tensile strength of 275 MPa).

6.3 Future work

Specific IMCs at the interface between Al 6063 and DP 600 might need to be checked with the method of XRD and TEM. Al 6063/DP 600 refill friction stir spot weldability needs to be confirmed when the tool is coated with a layer of material that might prohibit the adhesion issue. Furthermore, precise temperature measurement needs to be performed to understand the possibility of melting in the weld zone.

Appendix

1. Table 1: Base material compositions from chemistry analysis report [41]

	Al	Mg	Fe	Si	Mo	Cr	Cu	Mn	Zn	Nd	Zr	C
Al 6063	Bal.	0.49	0.2	0.39	<0.01	<0.01	0.02	0.03	<0.01	<0.01	<0.01	<0.01
Al 6463	Bal.	0.60	0.13	0.48	<0.01	0.02	0.07	0.08	<0.01	<0.01	<0.01	<0.01
ZEK 100	<0.01	Bal.	<0.01	<0.01	<0.01	<0.01	<0.01	0.01	1.3	0.2	0.25	<0.01
DP 600	0.05	<0.01	Bal.	0.35	0.01	0.02	0.03	1.8	0.01	<0.01	<0.01	0.09
Al 5754	Bal.	3.13	0.17	0.05	<0.01	<0.01	0.23	<0.01	<0.01	<0.01	<0.01	<0.01

2. AWS D8.1M:2007 standard

Based on the American Welding Society (AWS) D8.1M:2007 standard [42], the minimum recommended shear tension load for resistance spot welds in aluminum and steel can be calculated from the following equation:

$$ST = \frac{(-6.36E^{-7} \times S^2 + 6.58E^{-4} \times S + 1.674) \times S \times 4 \times t^{1.5}}{1000} \quad (Eq. 1)$$

Where S is the BM shear strength in MPa, and t is the sheet thickness in mm.

Reference

- [1] P. Kah, R. Suoranta, J. Martikainen and C. Magnus, "Techniques for joining dissimilar materials: metals and polymers", *Rev. Adv. Mater. Sci.* vol. 36, pp. 152-164, 2014.
- [2] P.L. Threadgill, A.J. Leonard, H.R. Shercliff and P.J. Withers, "FSW of aluminum alloys", *Int. Mater. Rev.*, vol. 54, pp. 49-93, 2009.
- [3] X.W. Yang, T. Fu, and W.Y. Li, "FSSW: A Review on Joint Macro- and Microstructure, Property, and Process Modelling," *Advances in Materials Science and Engineering*, 2014.
- [4] D.A. Wang and S.C. Lee, "Microstructures and failure mechanisms of friction stir spot welds of aluminum 6061-T6 sheets," *J. Mater. Process. Technol.*, vol. 186, no. 1–3, pp. 291–297, 2007.
- [5] C.J. Dawes and W.M. Thomas, "Friction stir process welds aluminum alloys", *Weld. J.*, vol. 75, pp. 41-45, 1996.
- [6] R.S. Mishra and Z.Y. Ma, "FSW and processing", *Mater. Sci. Eng.*, vol. 50, pp. 1-78, 2005.
- [7] Y. Kusuda, *Ind. Robot: An Int. J.*, vol. 40, pp. 208-212, 2013.
- [8] B.T. Gibson, D.H. Lammlein, T.J. Prater, W.R. Longhurst, C.D. Cox, M.C. Ballun, K.J. Dharmaraj, G.E. Cook and A.M. Strauss, "FSW: process, automation, and control", *J. Manuf. Processes*, vol. 16, pp. 56-73, 2014.
- [9] M. Haghshenas, S. Sahraeinejad, A. Abdel-Gwad, B. Gocke and A.P. Gerlich, "Dissimilar joining of automotive sheet materials by FSW", in: *CanWeld Conference*, Niagara Falls, Ontario, 2013.
- [10] C.M. Chen and R. Kovacevic, "Joining of Al 6061 alloy to AISI 1018 steel by combined effects of fusion and solid-state welding", *Int. J. Mach. Tools Manuf.* vol. 44, pp. 1205-1214, 2004.
- [11] "Honda Develops New Technology to Weld Together Steel and Aluminum and Achieves World's First Application to the Frame of a Mass-production Vehicle", <http://world.honda.com/news/2012/4120906Weld-Together-Steel-Aluminum/>
- [12] C.B. Smith, W. Crusan, J.R. Hootman, J.F. Hinrichs, R.J. Heideman and J.S. Noruk, "Friction Stir Welding In The Automotive Industry", *Aluminum 2001-Proceeding of the AMS 2001, Aluminum Automotive Joining Sessions*, 2001.
- [13] Y. Kusuda, "Honda develops robotized FSW technology to weld steel and aluminum and applied it to a mass-production vehicle", *Industrial Robot: An International Journal*, Vol. 40 Iss: 3, pp. 208 – 212, 2013.

- [14] M. Haghshenas, A. Abdel-Gwad, A.M. Omran, B. Gökçe, S. Sahraeinejad and A.P. Gerlich, "Friction-stir-weld assisted diffusion bonding of 5754 aluminum alloy to coated high strength steels", *Mater. Des.*, vol. 55, pp. 442-449, 2014.
- [15] Y.C. Chen and K. Nakata, "Effect of tool geometry on microstructure and mechanical properties of friction stir lap welded magnesium alloy and steel", *Mater. Des.*, vol. 30, pp. 3913-3919, 2009.
- [16] T. Liyanage, J. Kilbourne, A.P. Gerlich and T.H. North, "Joint formation in dissimilar Al alloy/steel and Mg alloy/steel friction stir spot welds", *Sci. Technol. Weld. Joining*, vol. 14, pp. 500-508, 2009.
- [17] M. Movahedi, A.H. Kokabi, S.M. Seyed Rehani and N. Najafi, "Effect of tool travel and rotation speeds on weld zone defects and joint strength of aluminum steel lap joints made by FSW", *Sci. Technol. Weld. Joining*, vol. 17, pp. 162-167, 2012.
- [18] Y.C. Chen and K. Nakata, "Effect of the surface state of steel on the microstructure and mechanical properties of dissimilar metal lap joints of aluminum and steel by FSW", *Metall. Mater. Trans. A*, vol. 39, pp. 1985-1992, 2008.
- [19] T. Gendo, K. Nishiguchi, M. Asakawa and S. Tanioka, in: *Proceedings of the SAE World Congress, Detroit (USA)*, and paper # 2007-01-1703, 2007.
- [20] R. Qiu, C. Iwamoto and S. Satonaka, "The influence of reaction layer on the strength of aluminum/steel joint welded by resistance spot welding", *Materials Charact.*, vol. 60, pp. 156-159, 2009.
- [21] W.M. Thomas, E.D. Nicholas and J.C. Needham, "FSW," International patent PCT/GB92102203 and Great Britain patent 9125978.8, 1991.
- [22] N.T. Nguyen, D. Y. Kim and H. Y. Kim, "Assessment of the failure load for an AA6061-T6 FSSW joint," *Proceedings of the Institution of Mechanical Engineers B: Journal of Engineering Manufacture*, vol. 225, no. 10, pp. 1746–1756, 2011.
- [23] L.E. Murr, G. Liu and J.C. McClure, "Dynamic recrystallization in FSW of aluminum alloy 1100", *J. Mater. Sci. Lett.*, vol. 16, pp. 1801-1803, 1997.
- [24] T. Rosendo, B. Parra and M.A.D. Tier, *et al.*, "Mechanical and microstructural investigation of friction spot welded AA6181-T4 aluminum alloy," *Mater. and Des.*, vol. 32, no. 3, pp. 1094–1100, 2011.
- [25] Z. Shen, X. Yang and S. Yang, *et al.*, "Microstructure and mechanical properties of friction spot welded 6061-T4 aluminum alloy," *Mater. and Des.*, vol. 54, pp. 766–778, 2014.
- [26] Z. Shen, X. Yang, Z. Zhang, L. Cui and T. Li, "Microstructure and failure mechanisms of refill friction stir spot welded 7075-T6 aluminum alloy joints," *Mater. and Des.*, vol. 44, pp. 476–486, 2013.

- [27] H. Badarinarayan, Q. Yang and S. Zhu, "Effect of tool geometry on static strength of friction stir spot welded aluminum alloy," *Int. J. of Mach. Tools and Manuf.*, vol. 49, no. 2, pp. 142–148, 2009.
- [28] W. Yuan, R.S. Mishra and S. Webb, *et al.*, "Effect of tool design and process parameters on properties of Al alloy 6016 friction stir spot welds," *J. of Mater. Process. Technol.*, vol. 211, no. 6, pp. 972–977, 2011.
- [29] Y.F. Sun, H. Fujii, N. Takaki and Y. Okitsu, "Microstructure and mechanical properties of mild steel joints prepared by a flat FSSW technique," *Mater. & Des.*, vol. 37, pp. 384–392, 2012.
- [30] M. Yamamoto, A. Gerlich, T.H. North and K. Shinozaki, "Cracking in dissimilar Mg alloy friction stir spot welds," *Science and Technology of Welding and Joining*, vol. 13, no. 7, pp. 583–592, 2008.
- [31] Y. Yan, D. Zhang, C. Qiu and W. Zhang, "Dissimilar FSW between 5052 aluminum alloy and AZ31 magnesium alloy", *Trans. of Nonferrous Metals Soc. of China*, vol. 20, pp. 619–623, 2010.
- [32] Z.H. Zhang, X.Q. Yang, J.L. Zhang, G. Zhou, X. Xu and B. Zou, "Effect of welding parameters on microstructure and mechanical properties of friction stir spot welded 5052 aluminum alloy," *Mater. & Des.*, vol. 32, no. 8-9, pp. 4461–4470, 2011.
- [33] H. Badarinarayan, Y. Shi, X. Li and K. Okamoto, "Effect of tool geometry on hook formation and static strength of friction stir spot welded aluminum 5754-O sheets," *Int. J. of Mach. Tools and Manuf.*, vol. 49, no. 11, pp. 814–823, 2009.
- [34] Y.H. Yin, A. Ikuta and T.H. North, "Microstructural features and mechanical properties of AM60 and AZ31 friction stir spot welds", *Mater. and Des.*, vol. 31, no. 10, pp. 4764–4776, 2010.
- [35] X. He, F. Gu, A. Ball, "A review of numerical analysis of friction stir welding", *Prog. Mater Sci.*, vol. 65, pp. 1-66, 2008.
- [36] X.W. Yang, T. Fu and W. Y. Li, "Friction Stir Spot Welding: A Review on Joint Macro- and Microstructure, Property, and Process Modelling", *Adv. Mater. Sci. and Eng.*, vol. 2014, pp. 11, 2014.
- [37] L.C. Campanelli, U.F. H. Suhuddin, A.I. S.Antonialli, J.F. dos Santos, N.G. de Alc[^]antara and C. Bolfarini, "Metallurgy and mechanical performance of AZ31magnesiumalloy friction spot welds," *J. Mater. Process. Technol.*, vol. 213, no. 4, pp. 515–521, 2013.
- [38] D.H. Choia, B.W. Ahna, C.Y. Leec, Y.M. Yeonb, K. Songb and S.B. Junga, "Formation of intermetallic compounds in Al and Mg alloy interface during FSSW", *Proceedings of the 7th International Workshop on Advanced intermetallic and Metallic Materials, intermetallic*, vol. 19, no. 2, pp. 125-130, 2011.
- [39] M.P. Mubiayi and E.T. Akinlabi, "FSSW of Dissimilar Materials: An Overview", *Proceedings of the World Congress on Engineering and Computer Science, San Francisco, USA*, vol. 2, 2014.

- [40] Z. Shen, Y. Chen, M. Haghshenas A.P. Gerlich, "Role of welding parameters on interfacial bonding in dissimilar steel/aluminum friction stir welds", *Eng. Sci. and Technol., an Inter. J.*, vol. 18, pp. 270-277, 2015.
- [41] M. Melendez, W. Tang, C. Schmidt, J.C. McClure, A.C. Nunes and L.E. Murr, Tool Forces Developed During Friction Stir Welding, <http://ntrs.nasa.gov/archive/nasa/casi.ntrs.nasa.gov/20030071631>.
- [42] U. Suhuddin, V. Fischer, F. Kroeft and J. F. dos Santos, "Microstructure and mechanical properties of friction spot welds of dissimilar AA5754 Al and AZ31 Mg alloys", *Mater. Sci. & Eng. A*, vol. 590, pp. 384-389, 2014.
- [43] C. Schneider, T. Weinberger, J. Inoue, T. Koseki and N. Enzinger, "Characterization of interface of steel/magnesium FSW", *Sci. and Technol. of Weld. and Join.*, vol. 16, pp.100–107, 2011.
- [44] I. Chumak, K. W. Richter and H. Ehrenberg, "Redetermination of iron dialuminide, FeAl₂", *Acta Crystallogr. C*, vol. 66, pp. 9, 2010.
- [45] "GalvInfoNote #10: The role of aluminum in continuous hot-dip galvanizing", ILZRO-GalvInfo Centre, 2003.
- [46] J. Culcasi, P. Sere, C. Elsner and A. Di Sarli, "Relationship between texture and corrosion resistance in hot-dip galvanized steel sheets", *Surf. Coat. Technol.*, vol. 122, pp. 21–23, 1999.
- [47] P. Penner, L. Liu, A. Gerlich and Y. Zhou, "Dissimilar Resistance Spot Welding of Aluminum to Magnesium with Zn Coated Steel Interlayers", *Weld. J.*, vol. 93, pp. 225–231, 2014.